



**Michigan  
Technological  
University**

Michigan Technological University  
**Digital Commons @ Michigan Tech**

---

Dissertations, Master's Theses and Master's Reports

---

2022

# PROCESS DEVELOPMENT, PHYSICAL, AND ELECTRICAL CHARACTERIZATION OF LANGMUIR BLODGETT TROUGH DEPOSITED POLYANILINE

Mehdi Malekrah

*Michigan Technological University, mmalekra@mtu.edu*

Copyright 2022 Mehdi Malekrah

---

## Recommended Citation

Malekrah, Mehdi, "PROCESS DEVELOPMENT, PHYSICAL, AND ELECTRICAL CHARACTERIZATION OF LANGMUIR BLODGETT TROUGH DEPOSITED POLYANILINE", Open Access Dissertation, Michigan Technological University, 2022.

<https://doi.org/10.37099/mtu.dc.etr/1381>

Follow this and additional works at: <https://digitalcommons.mtu.edu/etr>



Part of the [Electronic Devices and Semiconductor Manufacturing Commons](#)

PROCESS DEVELOPMENT, PHYSICAL, AND ELECTRICAL  
CHARACTERIZATION OF LANGMUIR BLODGETT TROUGH DEPOSITED  
POLYANILINE

By

Mehdi Malekrah

A DISSERTATION

Submitted in partial fulfillment of the requirements for the degree of

DOCTOR OF PHILOSOPHY

In Electrical Engineering

MICHIGAN TECHNOLOGICAL UNIVERSITY

2022

© 2022 Mehdi Malekrah

This dissertation has been approved in partial fulfillment of the requirements for the Degree of DOCTOR OF PHILOSOPHY in Electrical Engineering.

Department of Electrical and Computer Engineering

Dissertation Advisor: *Dr. Paul L. Bergstrom*

Committee Member: *Dr. Durdu Guney*

Committee Member: *Dr. Andrew J. Gross*

Committee Member: *Dr. Smitha Rao Hatti*

Department Chair: *Dr. Glen E. Archer*

## **Dedication**

*To my beloved wife and son, Mozhi and Liam, and my dear parents, Mary and Manouchehr, whose pure love and support brought me to where I am today.*

# Table of Contents

List of Figures .....	vii
List of Tables .....	xiii
Author Contribution Statement.....	xiv
Abstract.....	xv
1. Introduction.....	1
1.1 Electroconductive Polymers.....	1
1.2 Polyaniline.....	3
1.3 Deposition Methods .....	6
1.3.1 Electrochemical deposition.....	6
1.3.2 Spin Coating Method.....	7
1.3.3 Drop Coating Method .....	7
1.3.4 Layer-by-Layer (LbL) Self-Assembly Method .....	8
1.4 LB-Trough.....	8
1.5 LB-Trough Polyaniline Films .....	14
1.6 Objectives.....	15
1.7 References .....	18
2. Characterization of Molecular Weight Impacts on Polyaniline Thin Film Deposition by Langmuir Blodgett Trough Processing.....	24
2.1 Introduction .....	24

2.2	Experimental .....	27
2.2.1	Preparation of PANi mixture with NMP plus chloroform as solvent: 28	
2.2.2	Preparation of PANi mixture with NMP as solvent: .....	28
2.2.3	Substrate preparation: .....	28
2.2.4	LB-trough deposition and pressure-area isotherm graphs: .....	29
2.3	Results and Discussion .....	32
2.3.1	FTIR: .....	33
2.3.2	Transfer ratio analysis .....	36
2.3.3	AFM: .....	41
2.3.4	Spectroscopic Ellipsometry: .....	43
2.3.5	Thickness and surface roughness analysis .....	47
2.3.6	Electrical characterization .....	49
2.4	Conclusions .....	52
2.5	Acknowledgements .....	53
2.6	References .....	54
3.	Electrical Characteristics and Reversible Aging Effects in Polyaniline Thin Films Deposited by Langmuir-Blodgett Trough.....	60
3.1	Introduction .....	60
3.2	Experimental .....	62
3.2.1	Polyaniline oxidative polymerization .....	63
3.2.2	PANi LB trough deposition .....	64
3.2.3	Doping.....	64

3.2.4	Electrical conductivity study.....	65
3.2.5	SEM images .....	67
3.3	Results and Discussion.....	67
3.4	Conclusions .....	80
3.5	Acknowledgements .....	81
3.6	References .....	82
4.	Conclusion and Future works .....	86
4.1	Conclusion.....	86
4.2	Future Work .....	88
A	Appendix.....	90
A.1	Cauchy parameterization to determine Polyaniline film thickness .....	90

## List of Figures

- Figure 1. 1 Schematic chemical structures of (a) undoped semiconducting polymer polyacetylene, (b) polyaniline (PANi) (leucoemeraldine base ((X=0)), emeraldine base ((X=0.5)), pernigraniline base ((X=1)). .....2
- Figure 1. 2 Chemical structure of diverse oxidation forms of PANi: (a) Pernigraniline Base, fully oxidized form. (b) Emeraldine Base, intermediate oxidized. (c) Leucoemeraldine Base, fully reduced form. (Molecular structure produced using ChemDraw Professional V19.0.1.28.) [after 31] .....4
- Figure 1. 3 Chemical structure of Emeraldine Base polyaniline and transformation to Emeraldine Salt by doping (protonation) with hydrochloric acid. (Molecular structure produced using ChemDraw Professional V19.0.1.28.) [after 31].....5
- Figure 1. 4 Langmuir-Blodgett Trough deposition system with deionized water subphase, (a) Schematic illustration of a LB-Trough deposition system with a Wilhelmy plate and barriers, (b) image of actual KSV-2000 LB-Trough deposition tool configured with a single sample-scale trough well. The numbered parts are: 1 and 2 are barriers, 3 is sample holder arm which drives the sample up and down in controlled speed in (mm/min), 4 indicating a balance which holding the platinum Wilhelmy plate with a hook. Wilhelmy plate is partially immersed in subphase. ....10
- Figure 1. 5 Isotherm (II-A-isotherm) graph produced on the KSV-2000 instrument illustrates various monolayer polyaniline film phases for MW=5 000 g.mol<sup>-1</sup> and NMP + Chloroform as solvent. Cartoons indicate: (b) gas phase, (c) liquid phase, (d) solid phase, and (e) multilayer phase of polymers with “head” and “tail”

configurations. (Isotherm data is collected using KSV-2000 Langmuir-Blodgett Trough tool) .....	12
Figure 1. 6 Schematic illustration of LB-Trough deposited film, (a) deposition of a floating monolayer on a solid substrate, (b) three types of deposited LB-Trough film based on the polymer orientation. The polymer cartoons indicate “head” and “tail” configurations. ....	13
Figure 2. 1 Polyaniline generic chemical structure. Three oxidation states understood for polyaniline: (X=1) corresponds to Leucoemeraldine, (X=0.5) corresponds to Emeraldine, and (X=0) corresponds to Pernigraniline. {Molecular structure produced using ChemDraw Professional V19.0.1.28.} .....	27
Figure 2. 2 Isotherm graph produced on the KSV-2000 instrument illustrating various phases of monolayer polyaniline film for MWs 5000, 50000, and 100000 g.mol <sup>-1</sup> and NMP + Chloroform as solvent. (Isotherm data is collected using KSV-2000 Langmuir-Blodgett Trough tool and plotted in Origin Pro 2019b.) .....	32
Figure 2. 3 Reflectance ATR-FTIR spectra of LB-PANi films for undoped (DI water subphase) at top and doped (2M HCL subphase) at the bottom, (a) 5000 g.mol <sup>-1</sup> , (b) 50000 g.mol <sup>-1</sup> , (c) 100000 g.mol <sup>-1</sup> , (d) 5000 g.mol <sup>-1</sup> , (e) 50000 g.mol <sup>-1</sup> , (f) 100000 g.mol <sup>-1</sup> . (Data is collected using Thermo Scientific Nicolet iS50R FT-IR and plotted in Origin Pro 2019b.) .....	36
Figure 2. 4 The transfer ratio of 45 strokes LB-trough EB PANi film for three molecular weights, two different recepies (NMP only and NMP+Chloroform as solvent) and	

two different subphase (DIW and 2M HCl) on silicon substrate. (a) MW 5000 g.mol<sup>-1</sup>, NMP solvent, DIW subphase. (b) MW 50000 g.mol<sup>-1</sup>, NMP solvent, DIW subphase. (c) MW 100000 g.mol<sup>-1</sup>, NMP solvent, DIW subphase. (d) MW 5000 g.mol<sup>-1</sup>, NMP solvent, 2M HCl subphase. (e) MW 50000 g.mol<sup>-1</sup>, NMP solvent, 2M HCl subphase. (f) MW 100000 g.mol<sup>-1</sup>, NMP solvent, 2M HCl. (g) MW 5000 g.mol<sup>-1</sup>, NMP+Chloroform solvent, DIW subphase. (h) MW 50000 g.mol<sup>-1</sup>, NMP+Chloroform Solvent, DIW subphase. (i) MW 100000 g.mol<sup>-1</sup>, NMP+Chloroform Solvent, DIW subphase. (j) MW 5000 g.mol<sup>-1</sup>, NMP+Chloroform Solvent, 2M HCl subphase. (k) MW 50000 g.mol<sup>-1</sup>, NMP+Chloroform solvent, 2M HCl subphase. (l) MW 100000 g.mol<sup>-1</sup>, NMP+Chloroform solvent, 2M HCl subphase. (Transfer ratio data is collected using KSV-2000 Langmuir-Blodgett Trough tool and plotted in Origin Pro 2019b.)

.....38

Figure 2. 5 AFM images of LB-trough PANi film, 45 strokes, molecular weight = 5000 g.mol<sup>-1</sup>, doped, NMP + chloroform solvent. Top row images are height sensor and bottom row images are amplitude error images for different scan sizes (a) 9 μm, (b) 3 μm, (c) 1 μm, (d) 500 nm (data collected by Bruker Dimension ICON AFM)..42

Figure 2. 6 AFM images of the 5000 g.mol<sup>-1</sup> LB-trough PANi film for the thickness measurement. (a) 2-dimensional image with a scan size of 17 μm. A step edge was made in the film using a sharp blade. (b) 3-dimensional perspective image. (c) Cross-section profile across the indicated dashed line in (a). (data collected by Bruker Dimension ICON AFM). .....43

Figure 2. 7 Measurement and fitting graph for the wavelength range 300 – 1500 nm, the sample model and fitting parameters with relative error for two different spots on the sample (data is collected by J.A. Woollam V-VASE ellipsometry and plotted in Origin Pro 2019b). .....	45
Figure 2. 8 LB-trough PANi 5000 g.mol <sup>-1</sup> MW film thickness and roughness AFM measurement according to number of layers and doping state: (a) AFM film thickness measurement (b) Root Mean Square (RMS) roughness AFM data for various area sizes 0.5, 1, 3, and 9 μm <sup>2</sup> . (Data is collected by Keithley 4200A-SCS parameter analyzer and plotted in Origin Pro 2019b).....	48
Figure 2. 9 Current–voltage graph with different levels of doping for 45 strokes LB-Trough deposited PANi films on interdigitated electrodes: (a) commercial 5000 g.mol <sup>-1</sup> emeraldine PANi, (b) oxidative synthesized emeraldine PANi (Data is collected by Keithley 4200A-SCS parameter analyzer with measurement resolution of ±0.2 μV, ±100 fA and plotted in Origin Pro 2019b).....	51
Figure 3. 1 Sketch of an interdigitated electrode array used in this study. Electrodes were fabricated in Cr/Au, 5nm/30nm thickness respectively on a 160 nm thermally grown oxide layer on silicon substrate: d = spacing between fingers and w = fingers overlay length.....	66
Figure 3. 2 Semi-log plot of the electrical conductivity versus hydrochloric molarity (neutral, 0.1, 0.5, 1, 1.5, 2, 2.5 M HCl) as a subphase of LB-Trough deposited PANi film on interdigitated electrodes (IDEs) .....	69

Figure 3. 3 The room-temperature electrical properties of 45 layers LB-Trough-deposited PANi film on interdigitated gold electrodes on a silicon substrate post-deposition doping process by dipping in acidic bath (HCl), (a) Conductivity variation as function of hydrochloric acid molarity and time, (b) current vs. voltage characteristics as function of dipping time: 1 min, 10 min, 2 h and 24 hr.....71

Figure 3. 4 SEM images of 45 layers LB-Trough-deposited PANi films on (a)(b) silicon substrates with 160 nm oxide layer, (c)(d) interdigitated electrodes (30-nm Au on 5-nm Cr) fabricated on a (100) Si substrate covered by 160 nm thermal oxide. Each electrode finger is 20- $\mu\text{m}$  wide and the gaps between the electrodes are 100- $\mu\text{m}$ . (a) undoped PANi film using neutral deionized water subphase (b)(c) doped PANi film using acidic subphase, 1.5 M HCl (d) doped PANi film using deionized water neutral subphase and acidic bath, 1.5 M HCl for 24 hr. The inset images show PANi film at the border of electrode.....72

Figure 3. 5 In-plane electrical conductivity versus the number of single layer LB-Trough transferred PANi film: (a) employing 1.5 M HCl subphase, (b) using neutral subphase for deposition and using 1.5 M HCl dipping bath for 24 h post deposition. The slopes on the graphs are 0.25 and 1 for the linear portion of the (a) and (b) graphs respectively.....74

Figure 3. 6 Electrical conductivity of 45 layers LB-Trough-deposited PANi film versus aging time for (a) employing 1.5 M HCl subphase, (b) using netral subphase for deposition and using 1.5 M HCl bath for doping.....77

Figure 3. 7 Response and recovery time of 45 layers LB-Trough-deposited PANi film to 0.1 M  $\text{NH}_4\text{OH}$ . Sample was dipped in 1.5 M HCl for the recovery process. ....79

## List of Tables

Table 2. 1 FTIR peak assignment of 45 layers LB-trough PANi EB ( $5000 \text{ g.mol}^{-1}$ ) for undoped and doped (2M HCl) thin films.....	34
Table 3. 1 Conductivity, carrier density, and mobility of HCl doped LB-Trough PANi films .....	76

## **Author Contribution Statement**

The manuscripts, figures and results of this dissertation, which is presented in 4 interdependent chapters, are derived from two submitted journal manuscripts which are under review. The manuscript submission details are provided below.

Mehdi Malekrah

The articles list:

- 1) M. Malekrah and P.L. Bergstrom, “Characterization of Molecular Weight Impacts on Polyaniline Thin Film Deposition by Langmuir Blodgett Trough Processing”, Under review in Thin Solid Films, March 2022
- 2) M. Malekrah and P.L. Bergstrom, “Electrical Characteristics and Reversible Aging Effects in Polyaniline Thin Films Deposited by Langmuir-Blodgett Trough”, Submitted to Synthetic Metals, March 2022

## Abstract

Conductive polymers have recently attracted a lot of attention in advanced technologies because of their unique characteristics. Among the conductive polymers, polyaniline (PANi) has been studied widely because of its environmental stability, simple processing, inexpensive source monomer, and, most importantly, its controllable wide conductivity range due to the doping (protonation) process. These characteristics of PANi make it a strong candidate for applications in numerous areas such as biosensors, transparent display, photovoltaic devices, batteries, and, more recently, flexible electronics. Even with the many studies that have been conducted in this field, however, future advances are still needed to optimize the processability, conductivity, and environmental stability of PANi through modification of polymerization conditions, deposition techniques, and doping processes for specific applications. This dissertation focuses on optimizing PANi thin film deposition using the Langmuir-Blodgett Trough (LB-Trough) technique. In this regard, the impact of the solvent composition for the mixture preparation, the PANi polymer chain molecular weight (5000, 50000, and 100000  $\text{g}\cdot\text{mol}^{-1}$ ), and the subphase chemistry have been investigated to explore the impact on the physical properties of the PANi film characteristics and processing. In addition, the electrical characteristics of the LB-Trough deposited PANi film using interdigitated electrodes by employing two methods of doping and electrical conductivity aging were studied. The results revealed the most promising thin-film quality with regard to film uniformity within a sample and from sample to sample and the reproducible nanometer-scale deposition across many samples when using the lowest molecular weight available, 5000  $\text{g}\cdot\text{mol}^{-1}$ , and employing NMP+chloroform as the

solvent. The film thickness measurement revealed a range between 1.1 and 2.2 nm per single-layer film thickness deposition. The highest conductivity measured was  $41 \text{ S.m}^{-1}$  for a 45 LB-Trough deposited PANi film using 1.5 M HCl as the doping source and a 24 h exposure time. Thirty days of electrical conductivity aging data in the lab environment determined a steep degradation in conductivity during the first five days after deposition before the sample reached its steady state. The redox reversibility testing demonstrated that 72% of the initial conductivity may be recovered after ten aging and recovery cycles.

# 1. Introduction

## 1.1 Electroconductive Polymers

In the 21st century era, polymers are everywhere, and they impact all aspects of our daily lives. Although there are natural polymers in nature, such as silk and rubber, most of the polymers we use are chemically synthesized by engineering methods. Some of the novel properties of engineered polymers are high strength for their low mass, resistance to corrosion, simple processing, and low cost [1, 2]. We can compare the properties of different polymers in many ways. For example, they are classified into organic and inorganic groups based on the atomic-level structure. While the former group polymers are made of carbon atoms in their backbone chain (e.g., polyethylene), the latter group has other elements in their backbone structure, such as silicone rubber, which has silicon and oxygen groups in the backbone chain [3]. In addition, polymers can be classified as either thermoplastics or thermosets based on their molecular structure and thermal behavior. Thermoplastics can be melted and molded at high temperatures and then hardened when cooled down to lower temperatures [1, 4]. On the other hand, thermoset polymers are rigid, and they become set to or cured at high temperatures and remain in that form indefinitely [1, 4].

Polymers also can be categorized based on their electrical conductivity properties. While the majority of the polymers are classified as insulators, certain types of them are electrically conductive. Alternating double and single bonds along the polymer chain are the key to conductive properties [2]. This feature of the polymer is known as conjugation. In a non-conjugated polymer, the electrons are unable to move freely between the atoms in



of magnitude or more through the doping process. For example, polyacetylene conductivity is  $\sim 10^{-10}$  S/cm in undoped form and can be increased to greater than  $4 \times 10^4$  S/cm when is doped with iodine, which is comparable with copper conductivity  $5.9 \times 10^5$  S/cm at room temperature [13]. Because of this, conductive polymers are also known as organic metals.

A study claimed that conducting polymers' broad potential and technical possibilities are still unknown [14]. One of the research areas in which organic metals have attracted researchers' attention in recent years is conducting nanoparticle materials. It is known that conventional nanometals, such as Au or Ag, are not highly conductive ( $\sim 10^{-6}$  and  $10^{-4}$  S/cm respectively), and only annealing at higher temperature ( $<100^\circ\text{C}$ ) will assist in increasing their conductivity to the metallic range but, in the process, the annealing will degrade their nanoscaled quantum character [14]. In contrast, organic nano metals show a much higher conductivity  $\sim 10^2$  S/cm, despite their nano-size [15].

## **1.2 Polyaniline**

Among the conductive polymers, polyaniline (PANi) is one of the most studied ones and is under interest in electronic devices because of its novel properties such as environmental stability, biocompatibility, low cost monomer, a simple doping process, and a wide range of conductivity [16, 17]. PANi was discovered by Ferdinand Runge in 1834 and was known as "aniline black" at that time [18]. Later, Henry Letheby studied acidic solutions of aniline with various oxidizing agents to produce blue-to-purple colors, representing different oxidation states and concentrations of the aniline, in 1862 [19]. It wasn't until 1912 that Green and Woodhead discovered that different aniline forms exhibited different electrical properties, from insulating to conducting [20]. The generic chemical structure of PANi is

shown in Figure 1.1b. Polyaniline has three reversible oxidation states with a specific backbone structure which is formed of various ratios between quinoid and benzoic rings. These are shown in Figure 1.2. In Perniganiline Base, which is the fully oxidized form of PANi, there are equal numbers of quinoid and benzoic rings. For Emeraldine Base PANi, which is the intermediate oxidized state, there is one quinoid ring for every three benzoic rings. The Leucoemeraldine Base of PANi which is the fully reduced form, there is no quinoid ring [21, 22].

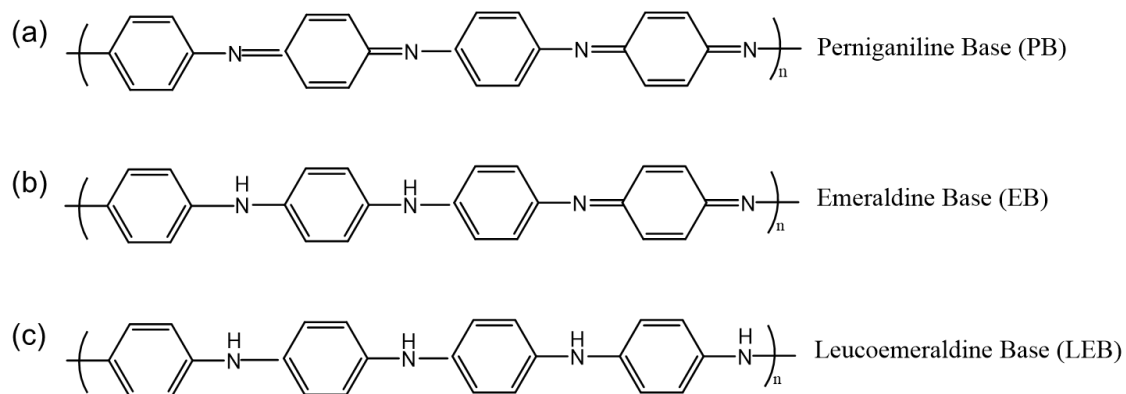


Figure 1. 2 Chemical structure of diverse oxidation forms of PANi: (a) Perniganiline Base, fully oxidized form. (b) Emeraldine Base, intermediate oxidized. (c) Leucoemeraldine Base, fully reduced form. (Molecular structure produced using ChemDraw Professional V19.0.1.28.) [after 31]

The emeraldine form of PANi is of primary interest in the semiconductor industry because its conductivity can be changed from an insulator ( $10^{-12} \text{ Scm}^{-1}$ ) in emeraldine base (undoped) form in blue color to a semiconducting polymer ( $10^{-4} - 10^{-2} \text{ Scm}^{-1}$ ) in the emeraldine salt (doped) form in green color [23]. The existence of the reactive group -NH- in the polymer chain, which is bonded to phenylene rings on either side, imparts chemical stability, relatively high conductivity, and the hydrophilic characteristics to the system [24,

25]. Emeraldine PANi has a shape that includes parts of imine (=N-) and amine (-NH-) nitrogen sites (Figure 1.2b).

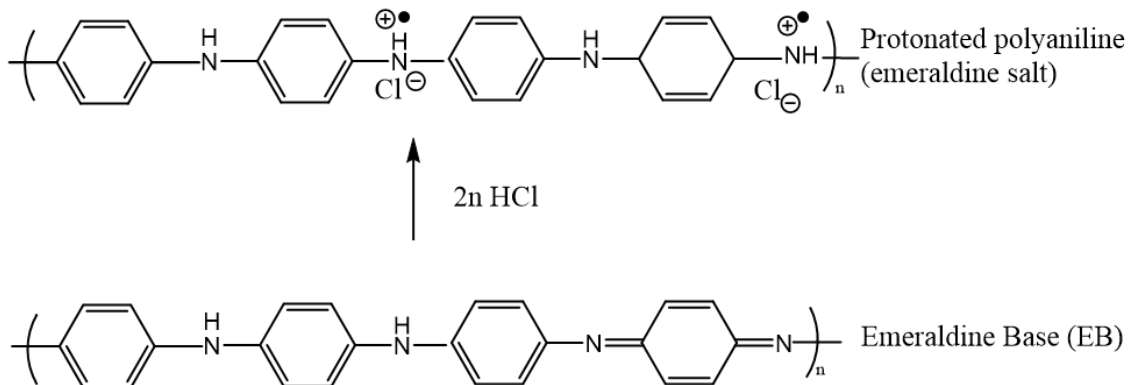


Figure 1. 3 Chemical structure of Emeraldine Base polyaniline and transformation to Emeraldine Salt by doping (protonation) with hydrochloric acid. (Molecular structure produced using ChemDraw Professional V19.0.1.28.) [after 31]

For the PANi doping process at presence of a protonic acid i.e., HCl imine sites are protonated to the bipolaron<sup>1</sup> state. Therefore, the PANi doping will be a protonation using a protonic acid i.e., HCl to add excess holes (p-type) to the electronic structure [26]. In the doping process, hydrochloric acid in reaction with polyaniline will remove the lone-pair of electrons from the double-bonded imine nitrogen atoms (Figure 1.3). As a result, some vacancies (holes) will be created in the  $\pi$ -electron orbital cloud. In fact, doping converts the imine sites (nitrogen atoms with a double bond) to iminium (nitrogen atoms with a positive charge) sites [17, 27]. In this process, HCl acid removes electrons from the PANi

<sup>1</sup> “In organic chemistry, a bipolaron is a molecule or part of a macromolecular chain containing two positive charges in a conjugated system.” (<https://en.wikipedia.org/wiki/Bipolaron>)

polymer imine sites in order to generate positive (holes) charge carriers, and creates both allowed states and available charge through the polymer chain [27, 28].

### **1.3 Deposition Methods**

Various techniques have been demonstrated for PANi thin film deposition, such as electrospinning [29], spin coating [30], thermal evaporation [31], layer-by-layer (LbL) self-assembly method [32], electrochemical deposition [33], and Langmuir-Blodgett trough (LB-trough) deposition [34-36]. Application drivers contribute to the choice of technique and impact the suitability of the resulting films. For example, while the electrochemical technique has a higher deposition rate compared to LB-trough, to achieve improved levels of film uniformity, crystallinity, and thickness control, the LB-trough technique is a better option [31] because of the unique control over the film thickness and molecular orientation [37]. A few previously demonstrated PANi thin film deposition methods are briefly explained below. An evaluation of each method is presented in comparison to the outcomes related to the LB-trough methodology.

#### **1.3.1 Electrochemical deposition**

In this method, in-situ oxidative polymerization of the monomer (aniline in this case) in a diluted acid (HCl or H<sub>2</sub>SO<sub>4</sub>) media takes place. PANi can be synthesized by three different electrochemical methods: (a) the galvanostatic technique that applies a constant current, (b) the potentiostatic technique with a constant voltage, and (c) the potentiodynamic technique in which current and voltage vary with a period. Regardless of which type of electrochemical deposition is used, the reactor vessel will consist of a three-electrode assembly that includes: (a) working electrode, (b) reference electrode, and (c) auxiliary

electrode. The electrodes usually are made of Pt, Ni, Au, or indium tin oxide (ITO) coated glass. The acid concentration will control the doping level of PANi polymer and depends on the type of polymerization in use; voltage or current can control the deposition rate of the thin film. Although ultra-thin PANi film can be achieved in this method, it is limited to a deposition only on conducting surfaces, and the thickness is sensitive to regions of electric field concentration, such as the edge of a patterned electrode area [35, 38].

### **1.3.2 Spin Coating Method**

This deposition technique is widely used for organic films in the semiconductor industry. In this method, a certain volume of the PANi polymer dissolved in a suitable solvent in a solution with a characterized viscosity and fluidic properties is applied onto a substrate, spinning at a speed balancing the kinetic centripetal forces with the viscous adhesion of the film to the underlying substrate. The viscosity of the solution, spinning speed, and time will define the film thickness performed on the substrate. After vaporization of the solvent in the solution, a solid thin film of polymer remains on the substrate [5, 31].

### **1.3.3 Drop Coating Method**

In this technique, PANi is dissolved in a suitable solvent and stirred for a required time to reach conditions for a homogenous mixture. The solution is filtered through a paper of appropriate porosity to eliminate undissolved polymer particles, and then a certain amount of the mixture is applied onto the clean surface of the substrate dropwise. The substrate will be left to air dry, or a vacuum chamber can be used to expedite the drying process. A thicker film can be formed by repeating this process [5, 31].

### **1.3.4 Layer-by-Layer (LbL) Self-Assembly Method**

In this technique, the target substrate is cleaned and placed on the bottom of the deposition bath. The container will be filled with deionized water, and the desired amount of PANi mixture will be spread on the water surface by pipetting. A single layer PANi film will be formed on top of the water in self-assembly order. A single layer PANi film will be deposited on the substrate by extracting the water from the container. These steps can be repeated to reach to a thicker film [5, 32].

## **1.4 LB-Trough**

The idea behind this technique may date back to the late 1700s when Benjamin Franklin used an oil droplet and let it spread to perform a monolayer on a pond. At that time, he did not understand the nature of a monolayer film on the water surface, but he found a relation between the oil volume and the area covered by oil on the water surface [39]. Many scientists investigated different aspects of this phenomenon afterward; however, Irving Langmuir was the one who showed amphiphilic films are monolayers with the hydrophilic part in contact with water surface and hydrophobic part, oriented straight up into the air. He won the chemistry Nobel prize for this discovery in 1932 [40]. A few years later, Katherine Blodgett, who was Irving Langmuir's student, showed that multilayer deposition is possible for amphiphilic molecules on a solid substrate.

The LB-trough deposition system consists of a hydrophobic trough (usually made of Teflon) which mostly is filled with deionized water as the subphase solution, two moveable barriers which, depending on the deposition type, can be hydrophilic or hydrophobic

(Figure 1. 4), and a Wilhelmy plate (made of Pt) which is used to measure surface pressure (mN/m),  $\Pi$ . The surface pressure is given by the relationship below:

$$\Pi = \gamma - \gamma_0$$

Where  $\gamma$  is the surface tension in the absence of a monolayer and  $\gamma_0$  is the surface tension with the monolayer present.

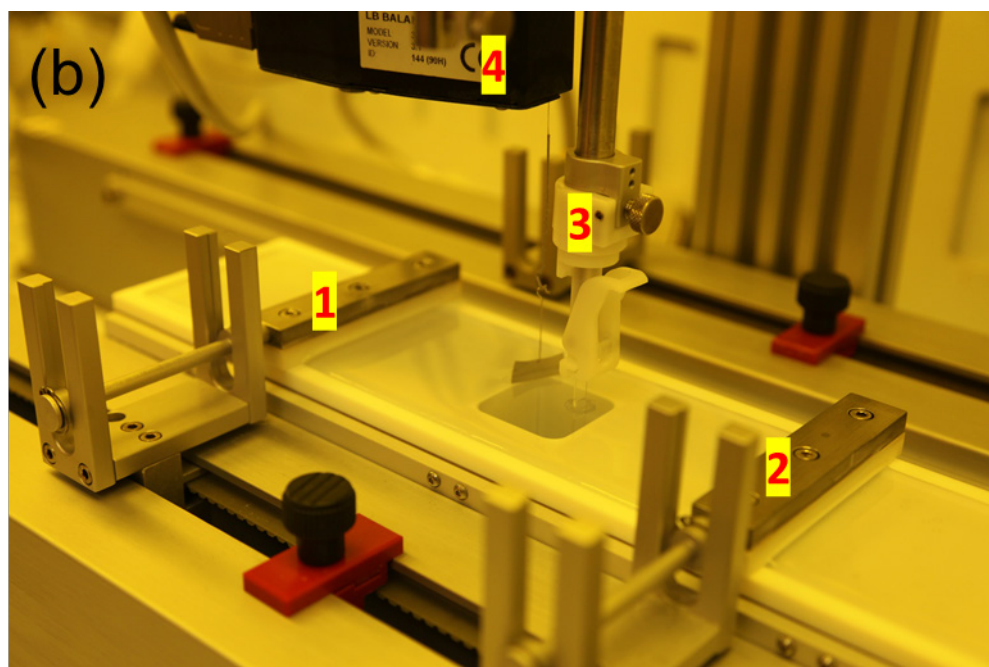
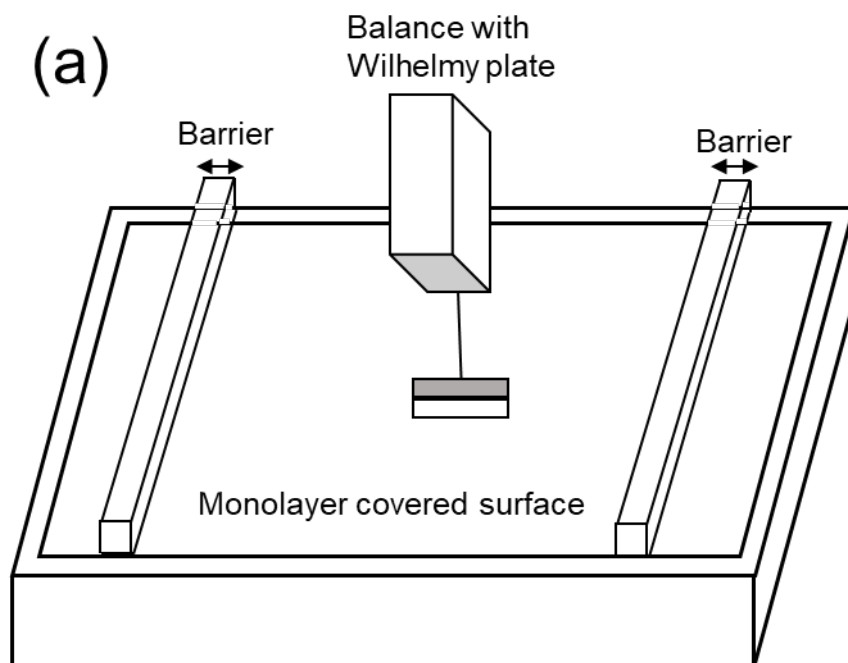


Figure 1. 4 Langmuir-Blodgett Trough deposition system with deionized water subphase, (a) Schematic illustration of a LB-Trough deposition system with a Wilhelmy plate and barriers, (b) image of actual KSV-2000 LB-Trough deposition tool configured with a single sample-scale trough well. The numbered parts are: 1 and 2 are barriers, 3 is sample holder arm which drives the sample up and down in controlled speed in (mm/min), 4 indicating a balance which holding the platinum Wilhelmy plate with a hook. Wilhelmy plate is partially immersed in subphase.

To prepare the tool for deposition, first the barriers are positioned as wide open, and an appropriate amount of amphiphilic mixture is spread over the subphase (DIW) surface by syringe or pipetting. By closing the barriers at a suitable rate ( $\leq 5$  mm/min) and monitoring the surface pressure and isotherm graph, deposition can begin after a solid phase of monolayer film is reached over the water surface. Different phases of the LB monolayer deposition are performed by squeezing the barriers to produce different surface pressures as shown in Figure 1. 5 on the next page.

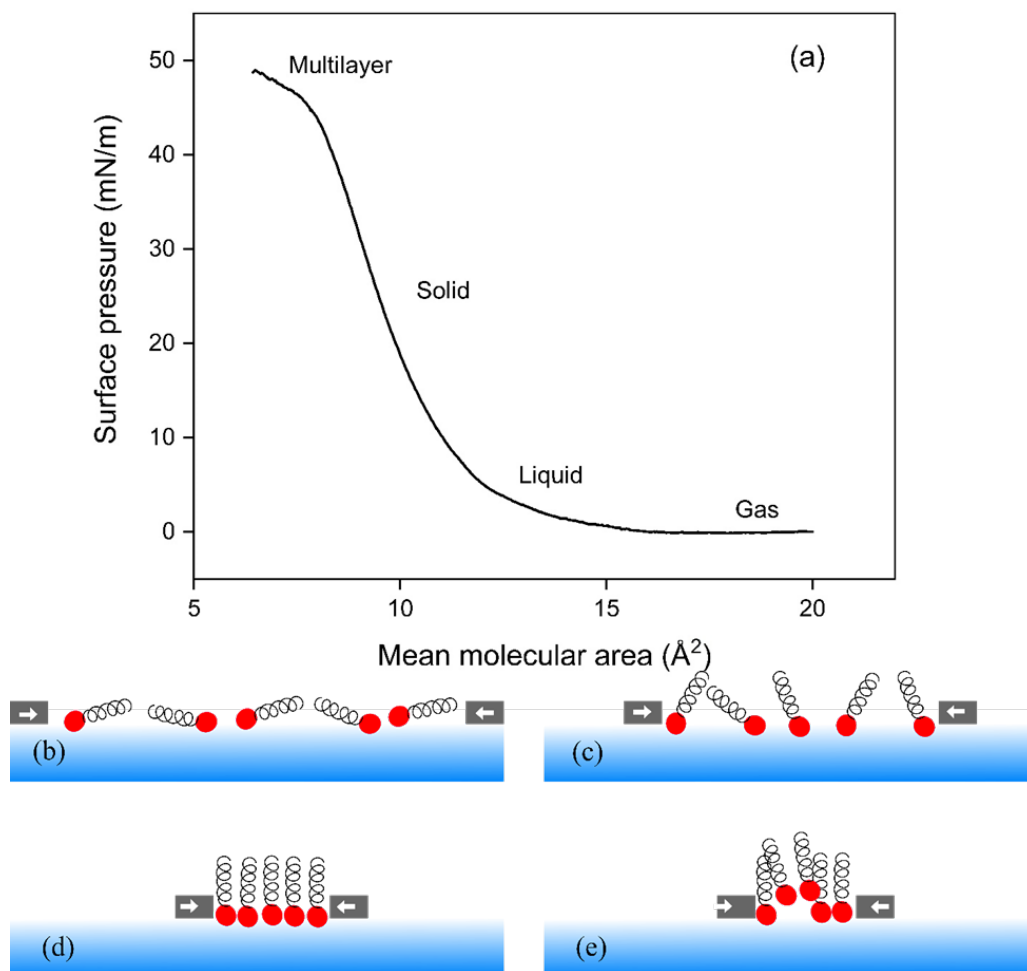


Figure 1. 5 Isotherm (II-A-isotherm) graph produced on the KSV-2000 instrument illustrates various monolayer polyaniline film phases for  $MW=5\ 000\ \text{g}\cdot\text{mol}^{-1}$  and NMP + Chloroform as solvent. Cartoons indicate: (b) gas phase, (c) liquid phase, (d) solid phase, and (e) multilayer phase of polymers with “head” and “tail” configurations. (Isotherm data is collected using KSV-2000 Langmuir-Blodgett Trough tool)

The LB deposition is traditionally carried out in the "solid" phase. The surface pressure is then high enough to ensure sufficient cohesion (continuity) in the monolayer, e.g., the attraction between the molecules in the monolayer is high enough so that the continuous monolayer does not fall apart or separate into domains during transfer of the film to the

solid substrate. This also ensures the buildup of homogeneous multilayers. Different kinds of LB multilayers can be produced and/or obtained by successive deposition of monolayers on the same substrate (Figure 1. 6).

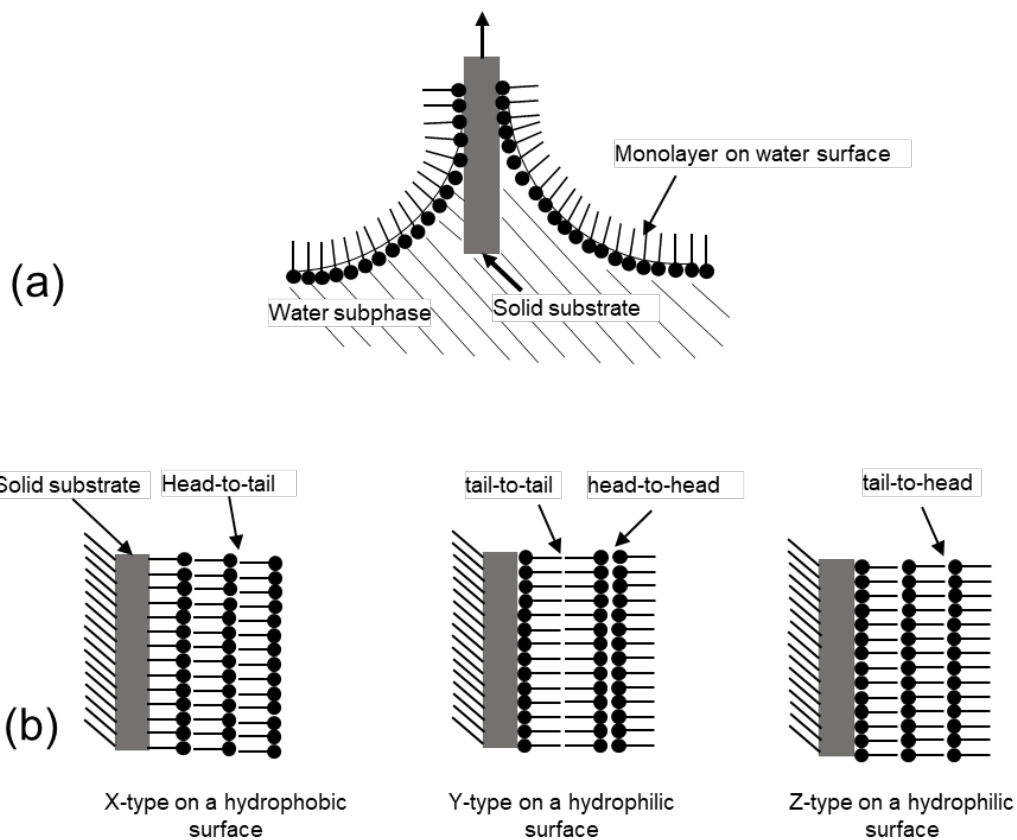


Figure 1. 6 Schematic illustration of LB-Trough deposited film, (a) deposition of a floating monolayer on a solid substrate, (b) three types of deposited LB-Trough film based on the polymer orientation. The polymer cartoons indicate “head” and “tail” configurations.

When the monolayer deposits only in the up or down direction. The multilayer structure is called either Z-type or X-type, respectively. In a Y-type multilayer LB-film, the monolayer deposits on the solid substrate in both the up and down deposition directions.

## **1.5 LB-Trough Polyaniline Films**

LB-Trough deposited PANi film processing has been of interest to a variety of research groups for two decades. Agbor and coworkers successfully deposited LB-Trough PANi film on silicon and glass substrates and used them as a gas sensor. He compared spinning, thermal evaporation, and LB-Trough deposition methods and demonstrated the highest sensitivity for his sensor out of LB-Trough PANi films [31, 41]. Ram, et al. deposited ordered LB-PANi films and studied the mean molecular area from the isotherm graph and the impact of the subphase temperature on the single-layer PANi film forming on the subphase [42, 43]. Suwa, et al. added a fatty acid (stearic acid) to the mixture preparation and introduced post-deposition treatments to remove the fatty acid from the film [44]. Goldenberg and coworkers used NMP (N-methyl-2-pyrrolidone) as the solvent and illustrated enhanced LB-PANi film quality based on voltammetric properties [45]. Huo, et al. used camphorsulfonic acid and dodecylbenzenesulfonic acid for the LB-PANi film doping and characterized the film using infrared and UV-vis spectroscopy [46]. Prabhakar and coworkers successfully deposited LB-PANi-stearic acid film onto ITO coated glass substrates and demonstrated the film functionality as a biosensor [34]. Bhullar, et al. illustrated PANi-ZnO nano-composite structure film using LB—Trough deposition and characterized the film by UV-Vis, Fourier transform infrared spectroscopy and atomic

force microscopy [47]. They showed a larger current range is achievable using the PANi-ZnO nanocomposite compared to LB-PANi film [47].

## 1.6 Objectives

Despite all the existing research on LB-PANi films, many open questions remain to resolve for this topic. For instance, even though a number of research groups studied the LB-PANi film deposition method and the mixture preparation on the film quality, not enough attention was paid to the impact of the molecular weight of the source PANi polymer material on the LB-PANi film quality and deposition yield. In addition, for the LB-Trough PANi film deposition type, while most of the past work reported a Z-type deposition [31, 35, 41, 43, 48], there are also a few groups that reported a Y-type deposition [34, 42, 49, 50]. The literature is silent on this discrepancy. Furthermore, while several studies focused on the doping process development and achieving a higher conductivity on LB-PANi film, there is no data in the literature regarding the aging effects on the electrical conductivity. Finally, there are some past studies on polyaniline aging in bulk material, but there exists no such study for LB-Trough thin films with a quasi-two-dimensional structure.

A deep study was completed in this dissertation to seek to fill the gaps in the knowledge and find answers for the stated questions above. The results of these investigations are summarized in the following chapters. Chapter 2 and Chapter 3 in this dissertation represent two journal papers submitted for publication addressing the questions of molecular weight impacts on LB-PANi film properties, and on electrical characterization and aging effects in ordered LB-PANi thin films.

In Chapter 2, LB-Trough methods are used to deposit commercially available PANi at three molecular weights (5000, 50000, and 100000 g.mol<sup>-1</sup>) emeraldine base PANi (EB-PANi) on an oxidized silicon substrate. The impact of the subphase acidity on the film deposition type and quality was investigated by monitoring the transfer ratio data. Fourier transform spectroscopy (FTIR), atomic force microscopy (AFM), and ellipsometry have been used for film characterization. The data showed the best quality and most successful LB-Trough deposition occurred for the lowest molecular weight (5000 g.mol<sup>-1</sup>) under test with an average film thickness of 1.1 – 2.2 nm per layer. Electrical characterization is also done using interdigitated electrodes (IDEs). Our data showed the highest uniform LB-trough PANi film quality based on the successful deposition, and the film roughness and morphology will be formed from the lowest molecular weight (5000 g.mol<sup>-1</sup>). While LB-Trough deposited commercial EB-PANi film did not show electrical conductivity upon doping, our synthesized EB-PANi source material (oxidative polymerization) became highly conductive (41 S/m) as a result of subphase-based or post-deposition protonation.

In Chapter 3, the electrical characterization of the LB-PANi film was investigated using IDEs and under two different doping methods. The electrical conductivity aging was studied for 30 days post-deposition for each sample. Scanning electron microscopy (SEM) was used for the morphology and molecular structure studies of the PANi film. Hall effect measurement was also performed to collect more electronic properties data such as carrier mobility and carrier density. Our LB-Trough deposited PANi film on IDEs was tested for reversibility and redox cycling as an application demonstration. A 1.5 M HCl was used as the protonic acid and 0.1 M NH<sub>4</sub>OH for the oxidizer. The 10 times redox cycling

reversibility data revealed that %72 of the initial conductivity was recovered for LB-Trough deposited PANi film.

In Chapter 4, the demonstration of LB-PANi films applied to biochemical and electrochemical sensing is explored. The strong sensitivity of the PANi film to protonation state allows for a highly sensitive pH sensor to be considered. Binding a biochemical antigen protein to the LB-PANi surface enables the film to serve as a sensor for nonreversible binding events between antigen and antibody molecules when and if the binding events inhibit the transfer of charge in the interdigitated electrode arrays [51, 52].

## 1.7 References

1. Brinson, H.F. and L.C. Brinson, *Polymer engineering science and viscoelasticity*. An introduction, New York, Springer, 2008.
2. Das, T.K. and S. Prusty, *Review on conducting polymers and their applications*. Polymer-plastics technology and engineering, 2012. **51**(14): p. 1487-1500.
3. Baeriswyl, D., et al., *Conjugated conducting polymers*. Vol. 102. 2012: Springer Science & Business Media.
4. Siracusa, V., et al., *Biodegradable polymers for food packaging: a review*. Trends in Food Science & Technology, 2008. **19**(12): p. 634-643.
5. Beygisangchin, M., et al., *Preparations, properties, and applications of polyaniline and polyaniline thin films—A review*. Polymers, 2021. **13**(12): p. 2003.
6. Conwell, E., *Transport in trans-polyacetylene*. IEEE transactions on electrical insulation, 1987(5): p. 591-627.
7. Heeger, A. J., S. Kivelson, J. R. Schrieffer, and W. P. Su. "Rev. Mod. Phys." (1988): 781.
8. Ramanathan, K., et al., *Application of polyaniline-Langmuir-Blodgett films as a glucose biosensor*. Materials Science and Engineering: C, 1995. **3**(3-4): p. 159-163.
9. Kukla, A., Y.M. Shirshov, and S. Piletsky, *Ammonia sensors based on sensitive polyaniline films*. Sensors and Actuators B: Chemical, 1996. **37**(3): p. 135-140.
10. Huang, J., et al., *Nanostructured polyaniline sensors*. Chemistry—A European Journal, 2004. **10**(6): p. 1314-1319.
11. Dhawan, S., et al., *Application of conducting polyaniline as sensor material for ammonia*. Sensors and Actuators B: chemical, 1997. **40**(2-3): p. 99-103.

12. Liu, Z., et al., *Polyaniline/TiO<sub>2</sub> solar cells*. Synthetic metals, 2006. **156**(9-10): p. 721-723.
13. Epstein, A.J., et al., *Inhomogeneous disorder and the modified Drude metallic state of conducting polymers*. Synthetic metals, 1994. **65**(2-3): p. 149-157.
14. Braun, E., et al., *DNA-templated assembly and electrode attachment of a conducting silver wire*. Nature, 1998. **391**(6669): p. 775-778.
15. Wessling, B., *Conductive polymers as organic nanometals*, in *Handbook of nanostructured materials and nanotechnology*. 2000, Elsevier. p. 501-575.
16. MacDiarmid, A., et al., *Polyaniline: a new concept in conducting polymers*. Synthetic Metals, 1987. **18**(1-3): p. 285-290.
17. Sengupta, P.P. and B. Adhikari, *Influence of polymerization condition on the electrical conductivity and gas sensing properties of polyaniline*. Materials Science and Engineering: A, 2007. **459**(1-2): p. 278-285.
18. Rasmussen, S.C., *The early history of polyaniline: discovery and origins*. Substantia, 2017. **1**(2).
19. Letheby, H., *XXIX.—On the production of a blue substance by the electrolysis of sulphate of aniline*. Journal of the Chemical Society, 1862. **15**: p. 161-163.
20. Green, A.G. and A.E. Woodhead, *CXVII.—Aniline-black and allied compounds. Part II*. Journal of the Chemical Society, Transactions, 1912. **101**: p. 1117-1123.
21. Michira, I., et al. *Synthesis, characterisation of novel polyaniline nanomaterials and application in amperometric biosensors*. in *Macromolecular symposia*. 2007. Wiley Online Library.

22. Masters, J., et al., *Polyaniline: allowed oxidation states*. Synthetic Metals, 1991. **41**(1-2): p. 715-718.
23. Rajapakse, R., A.C. Perera, and H. Premasiri, *Polyaniline retained glass templates as sensors for acidic/basic and/or redox gases*. Journal of the National Science Foundation of Sri Lanka, 2010. **28**(4).
24. Bhullar, G.K., R. Kaur, and K. Raina, *Hybrid polyaniline–TiO<sub>2</sub> nanocomposite Langmuir–Blodgett thin films: Self-assembly and their characterization*. Journal of Applied Polymer Science, 2015. **132**(5).
25. Gurunathan, K. and D.C. Trivedi, *Studies on polyaniline and colloidal TiO<sub>2</sub> composites*. Materials Letters, 2000. **45**(5): p. 262-268.
26. Pouget, J., et al., *X-ray structure of polyaniline*. Macromolecules, 1991. **24**(3): p. 779-789.
27. Khalid, M., A.M.B. Honorato, and H. Varela, *Polyaniline: synthesis methods, doping and conduction mechanism*. 2018, IntechOpen London, UK:.
28. MacDiarmid, A.G. and A.J. Epstein, *Secondary doping in polyaniline*. Synthetic Metals, 1995. **69**(1-3): p. 85-92.
29. Rozemarie, M., et al. *Electrospun Based Polyaniline Sensors—A Review*. in *IOP Conference Series: Materials Science and Engineering*. 2017. IOP Publishing.
30. Farag, A., A. Ashery, and M.A. Rafea, *Optical dispersion and electronic transition characterizations of spin coated polyaniline thin films*. Synthetic metals, 2010. **160**(1-2): p. 156-161.
31. Agbor, N., M. Petty, and A. Monkman, *Polyaniline thin films for gas sensing*. Sensors and Actuators B: Chemical, 1995. **28**(3): p. 173-179.

32. Zhang, T., et al., *Engineering crystalline quasi-two-dimensional polyaniline thin film with enhanced electrical and chemiresistive sensing performances*. Nature communications, 2019. **10**(1): p. 1-9.
33. Conroy, K.G. and C.B. Breslin, *The electrochemical deposition of polyaniline at pure aluminium: electrochemical activity and corrosion protection properties*. Electrochimica Acta, 2003. **48**(6): p. 721-732.
34. Prabhakar, N., Z. Matharu, and B. Malhotra, *Polyaniline Langmuir–Blodgett film based aptasensor for ochratoxin A detection*. Biosensors and Bioelectronics, 2011. **26**(10): p. 4006-4011.
35. Zhang, J., et al., *Polyaniline Langmuir–Blodgett films: formation and properties*. Physical Chemistry Chemical Physics, 2009. **11**(18): p. 3490-3496.
36. Chen, C.-W., J.-H. Yeh, and T.-J.J.T.S.F. Liu, *Stable Langmuir–Blodgett film deposition of polyaniline and arachidic acid*. 2007. **515**(18): p. 7299-7306.
37. Gupta, V., et al., *Controlling molecular order in " hairy-rod" langmuir-blodgett films: A polarization-modulation microscopy study*. Science, 1994. **265**(5174): p. 940-942.
38. Prasad, K.R. and N. Munichandraiah, *Electrochemically deposited crystalline thin film of polyaniline on nickel for redox reactions at positive potentials*. Synthetic metals, 2002. **130**(1): p. 17-26.
39. Franklin, B., W. Brownrigg, and M. Farish, *Of the stilling of waves by means of oil. Extracted from sundry letters between Benjamin Franklin, LL. DFRS William Brownrigg, MDFRS and the Reverend Mr. Farish*. Philosophical Transactions (1683-1775), 1774: p. 445-460.

40. Langmuir, I., *The constitution and fundamental properties of solids and liquids. II. Liquids*. Journal of the American chemical society, 1917. **39**(9): p. 1848-1906.
41. Agbor, N., et al., *Langmuir-Blodgett films of polyaniline*. Synthetic metals, 1993. **57**(1): p. 3789-3794.
42. Ram, M., N. Sundaresan, and B. Malhotra, *Langmuir-Blodgett films of processable polyaniline*. The Journal of Physical Chemistry, 1993. **97**(45): p. 11580-11582.
43. Ram, M. and B. Malhotra, *Preparation and characterization of Langmuir-Blodgett films of polyemeraldine base*. Polymer, 1996. **37**(21): p. 4809-4813.
44. Suwa, T., et al., *Preparation and evaluation of polyaniline LB films*. Molecular Crystals and Liquid Crystals Science and Technology. Section A. Molecular Crystals and Liquid Crystals, 1994. **255**(1): p. 45-54.
45. Goldenberg, L., M. Petty, and A. Monkman, *A Comparative Study of the Electrochemical Properties of Dip-Coated, Spun, and Langmuir-Blodgett Films of Polyaniline*. Journal of the Electrochemical Society, 1994. **141**(6): p. 1573-1576.
46. Huo, L., et al., *Preparation and characterization of doped polyaniline films*. Thin Solid Films, 1999. **350**(1-2): p. 5-9.
47. Bhullar, G.K., R. Kaur, and K. Raina, *Growth, Morphology, and Electrical Characterization of Polyaniline-ZnO Nano-composite Langmuir-Blodgett Thin Films*. Journal of Electronic Materials, 2015. **44**(10): p. 3422-3429.
48. Matharu, Z., et al., *Polyaniline Langmuir- Blodgett film based cholesterol biosensor*. Langmuir, 2007. **23**(26): p. 13188-13192.
49. Dhanabalan, A., et al., *A Study of Langmuir and Langmuir- Blodgett Films of Polyaniline*. Langmuir, 1997. **13**(16): p. 4395-4400.

50. Cheung, J. and M. Rubner, *Fabrication of electrically conductive Langmuir-Blodgett multilayer films of polyaniline*. *Thin Solid Films*, 1994. **244**(1-2): p. 990-994.
51. Dhand, C., et al., *Polyaniline-based biosensors*. *Nanobiosensors in disease diagnosis*, 2015. **4**: p. 25.
52. Zare, E.N., et al., *Progress in Conductive Polyaniline-Based Nanocomposites for Biomedical Applications: A Review*. *Journal of medicinal chemistry*, 2019.

## **2. Characterization of Molecular Weight Impacts on Polyaniline Thin Film Deposition by Langmuir Blodgett Trough Processing**

### **2.1 Introduction**

The formation of uniform nanometer-thick conducting thin films, by depositing of single- and multilayers of conducting polymers, attracted researchers' attention during the last two decades. However, the deposition of such an ultrathin film is not a trivial challenge because of processing complexities of the well-known conducting polymers, such as polypyrrole, polythiophene and polyaniline (PANi). Although electrochemical deposition is a known technique for depositing such an ultrathin film, it will limit the deposition only to conducting substrates and produces nonuniformities in film characteristics based on electric field densities at film boundaries. The electrochemical deposition also is not a best option when the film surface roughness is a key quality factor, and a smoother film is desired i.e., in biosensors applications [1]. The other alternative deposition methods with ultrathin film thickness control are, photochemical synthesis, thermal evaporation [2], spin coating[3], electrospinning[4], and Langmuir-Blodgett Trough (LB-Trough) [5]. The latter technique, which is the focus of this paper, has proven results of nanometer control of the film thickness, quasi-two-dimensional (q2D) film structure, low production cost, and capability as an area scalable technique for the semiconductor industry [6-8].

Among the conducting polymers, PANi attracts additional interest due to its electrical conductivity, environmental stability, and significant redox behavior which is fully reversible. The generic chemical structure of PANi is shown in Figure 2. 1 below. Three

different oxidation states are understood for PANi, (Figure 2. 1) X=1 corresponds to leucoemeraldine, which is the reduced form, X=0.5 for emeraldine, which is the intermediate oxidation state of PANi, and X=0 for pernigraniline, which is fully oxidized form [9, 10]. The emeraldine form of PANi is of primary interest in the semiconductor industry because its conductivity can be modulated from an insulator ( $10^{-12} \text{ Scm}^{-1}$ ) in emeraldine base (undoped) to a semiconducting polymer ( $10^{-4} - 10^{-2} \text{ Scm}^{-1}$ ) in the emeraldine salt (doped) form [11]. The existence of the reactive group -NH- in the polymer chain, which is bonded to phenylene rings on either side, imparts chemical stability, relatively high conductivity, and the amphiphilic characteristics to the PANi chain which is a key factor for LB-Trough deposition technique [12, 13].

It is known that structural disorder in conductive thin film polymers slows down the charge transport, thus degrades electronic device performance [14]. A promising technique to achieve a longer-range charge transport is to align the linear conducting polymer chains into q2D crystalline films [6, 15]. Researchers have shown that PANi LB-trough film exhibits q2D film properties [8]. This makes PANi LB-trough film a strong candidate for two-dimensional structured devices and ultrasensitive sensors [5, 16].

A number of studies have focused on the PANi LB-Trough film deposition and characterization in the past. Agbor deposited PANi LB films on the interdigitated electrodes and used them as Ammonia gas sensor [2]. Chen, et al. used atomic force microscopy to measure surface roughness of polyaniline for different ratios of arachidic

acid in the mixture [17]. Goldenberg compared the electrochemical properties of dip-coated, spun, and LB-trough PANi thin film and showed LB films have distinguished voltametric properties and shown that LB films pose the best results among the other techniques [18]. Riul and coworkers studied LB-trough PANi film fabrication process by comparing ten different mixture preparation recipes using functionalized acids such as camphorsulfonic, and toluenesulfonic acids and organic solvents in various ratios [19]. Zhang, et al. showed long-range molecular ordering, quasi-two-dimensional (q2D), for PANi film deposition from air-water interface and achieving lateral conductivity up to  $160 \text{ Scm}^{-1}$  using hydrochloric acid protonation [6]. While most of the previous studies on LB-Trough PANi film reported Z-type (upward) deposition, there are a few groups have reported Y-type deposition (up- and downward) [5, 20-22]. In this study, we seek to understand the reason for this discrepancy in the literature, utilizing two of the most commonly used recipes for the mixture preparation and different subphase conditions in our investigation.

In all previous studies on LB-Trough PANi film deposition, aniline polymerization techniques such as oxidative, ultrasound-assisted, or electrochemical are used as the polymer source while polyaniline is commercially available in different forms, molecular weights, and oxidation states. In addition, it is shown in literature that higher molecular weights of PANi improves the lateral conductivity in electrochemically deposited films [23, 24], but there is no such data in literature for the LB-Trough deposited PANi film to investigate the Molecular Weight's impact on the conductivity or other properties of the

film such as uniformity, thickness, surface roughness, or air-water isotherm graphs. In this study, three different commercial molecular weights (5000, 50000, and 100000 g.mol<sup>-1</sup>) of emeraldine base PANi in powder forms are used to deposit on oxidized silicon substrates to fill this gap in the knowledge. In addition, characterization techniques such as attenuated total reflection – Fourier transform infrared spectroscopy (ATR-FTIR), ellipsometry, atomic force microscopy (AFM), and interdigitated electrodes for the conductivity are employed to perform a physical and electrical characterization analysis on LB-Trough PANi film.

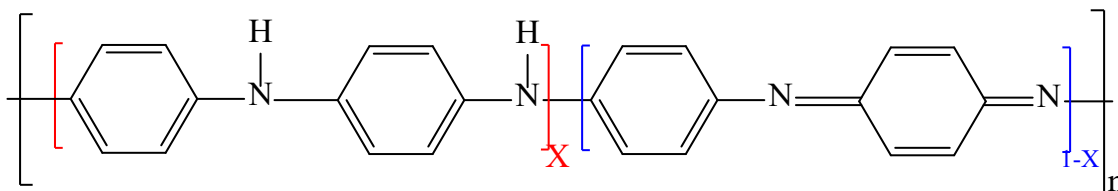


Figure 2. 1 Polyaniline generic chemical structure. Three oxidation states understood for polyaniline: ( $X=1$ ) corresponds to Leucoemeraldine, ( $X=0.5$ ) corresponds to Emeraldine, and ( $X=0$ ) corresponds to Pernigraniline. {Molecular structure produced using ChemDraw Professional V19.0.1.28.}

## 2.2 Experimental

**Material List:** The three molecular weights of Polyaniline Emeraldine Base 5000, 50000, and 100000 g.mol<sup>-1</sup> in powder form, chloroform (CHCl<sub>3</sub>) anhydrous  $\geq 99\%$ , containing 0.5 – 1.0% ethanol as a stabilizer, 1-Methyl-2-pyrrolidinone (C<sub>5</sub>H<sub>9</sub>NO) anhydrous 99.5%, known as NMP, and acetic acid (C<sub>2</sub>H<sub>4</sub>O<sub>2</sub>) reagent plus  $\geq 99\%$ , were purchased from Sigma Aldrich and used as received. Hydrochloric acid (HCl) A144C-212 certified ACS plus 36.5 to 38%, Whatman filter papers grade 4 with pore size 20 – 25  $\mu\text{m}$  were purchased from Fisher Scientific.

### **2.2.1 Preparation of PANi mixture with NMP plus chloroform as solvent:**

In this recipe, first a mixture of 1:10 by weight acetic acid: polyaniline was prepared. Then, 0.1 mg of the mixture is dissolved into 10 ml of solvent and ultrasonicated for 30 minutes using an Ultrasonic Power (Model 5300) by adjusting the power intensity and modulation frequency at 50%. The solvent used in this procedure is a mixture of chloroform: NMP in a 1:5 volume ratio. Finally, the filter paper is used to eliminate undissolved PANi particles. The polyaniline concentration in this recipe is around 0.01 mg/ml. The final mixture color is light blue; it is stored at room temperature to be used within 48 hours of preparation. A longer storage period will result in some degradation issues [25]. This recipe was demonstrated by Agbor, et al. for the first time in 1993 [26].

### **2.2.2 Preparation of PANi mixture with NMP as solvent:**

For the second recipe under consideration, acetic acid is added to polyaniline-EB powder in 1:10 by weight ratio, then NMP is used as the only solvent agent to make a 0.08 mg/ml concentration, and ultrasonicated for 30 minutes with the same settings. Again, the filter paper is used to separate undissolved PANi particles. The final mixture color is dark blue in this case because of a higher concentration. In this recipe, a lower volume of solvent is used. The mixture is stored in ambient conditions and used within 48 hours of preparation. This recipe was used by Dehanabalan, et al. for the first time in 1997 [20].

### **2.2.3 Substrate preparation:**

For the substrate, a 100 mm Si (100) single side polished wafer with p-type (Boron) doping and a resistivity 9.6–14.4  $\Omega/\text{cm}$  is used. Standard RCA SC-1 process cleaning [27] was employed for the Si wafers before producing a thermally grown silicon dioxide layer of

160 ± 5 nm at 1100 °C using a Mellen Clamshell furnace under dry environment and 3 SLM O<sub>2</sub> flow for two hours. Spectroscopic ellipsometry (J.A. Woollam V-VASE) was utilized to characterize the oxide layer film thickness over the Si wafer in a minimum of 5 locations. The silicon wafer was then spin-coated with a photoresist (Shipley 1827) to protect the sample's surface from debris contamination before dicing to the test die dimensions (5 mm × 20 mm). A Microautomation MA1000 dicing tool was used, and test die were stored in a dry box under nitrogen gas flow at ambient temperature. To prepare each substrate for deposition, a standard solvent cleaning including Acetone 3 min, Isopropyl alcohol (IPA) 3 min, followed by DIW rinse, and nitrogen dry was used to strip the photoresist and particles contaminations from substrate's surface. For the last step in the preparation, Piranha cleaning using H<sub>2</sub>SO<sub>4</sub>: H<sub>2</sub>O<sub>2</sub> in 3:1 volume ratio for 10 min was performed to remove all organic residual contamination from the substrate's surface and increase hydrophilic properties by hydroxylating the surface. The piranha cleaning process is performed immediately prior to LB-trough deposition to maximize the benefit from the substrate surface's hydrophilic properties.

#### **2.2.4 LB-trough deposition and pressure-area isotherm graphs:**

For the Langmuir-Blodgett trough deposition, a KSV-2000 tool has been used. The trough is made of Teflon (hydrophobic), and barriers are made of Delrin (hydrophilic) to prevent any monolayer's leakage from beneath the barriers. Before each run, the trough and barriers were washed with odor/color free detergent and rinsed, followed by IPA cleaning and a rinse with DIW. The tool was installed in a chemical processing bench in the cleanroom environment. For the subphase, DIW is used and surface pressure is measured using a Wilhelmy plate. In this method, the Wilhelmy plate with a known perimeter is partially

immersed in the subphase, and the force toward the plate is measured and converted into surface tension in mN/m regarding the plate's dimension. To clean the Wilhelmy plate, a Bernzomatic propane torch was used to burn and flash all remaining organic materials on the plate surface from previous runs. The Wilhelmy plate should show hydrophilic properties on the surface; otherwise, oxygen plasma cleaning can be applied.

For the film deposition, the trough is filled by DIW when barriers are in their wide-open position. Before adding the mixture, barriers are closed once, and the aspirator collects any potential contamination from the DIW surface. Barriers open again, a sample is placed on the deposition arm and dipped into DIW before applying the PANi mixture. The mixture dispersed on the water surface using a 20-200  $\mu\text{l}$  Thermo fisher manual pipette. The required amount of the mixture can vary depending on the recipe and the target number of deposition layers. Then, barriers are closed at a 5 mm/min pace, and a monolayer isotherm graph is performed in the KSV control software (Figure 2. 2). Depending on the material and recipe is used, a repeated isotherm graph test may be necessary to achieve a reproducible trace. Figure 2. 2 clearly shows the mean molecular area differences of repeated units for three molecular weights tested here.

The isotherm graph shows that the initial surface pressure increase took place around 8  $\text{\AA}/\text{r.u}$  for the 5000  $\text{g.mol}^{-1}$  molecular weight (Figure 2. 2). This is called a phase transition from gas to liquid based on the distances between the molecules for the Langmuir film which starts to form at the air water interface [28, 29]. This phase transition happened on

a higher range around 15 and 20 Å/r.u for 50000 and 100000 g.mol<sup>-1</sup> molecular weights respectively, which was expected because they have a longer polymer chain. Further squeezing the barriers will result surface pressure increase more rapidly. During this phase, is also known as solid phase, the polymer molecules will interact more closely and start to create packed organized two-dimensional islands. Nicolini's group has shown this clearly using Brewster angle microscopy (BAM) technique in the past [28]. More compression of the barriers resulted a single layer well packed quasi-two-dimensional PANi film take place at the air water interface. Continuing to close the barriers, when the surface pressure reached to 45 mN/m, the quasi-two-dimensional film started to collapse as the monolayers slid on top of each other resulting in multilayer films at the air-water interface, which can be visibly observed without magnification. This phase transition is known as the multilayer phase[28]. For the film deposition in this study, the surface pressure was set to 30 mN/m as reported previously in the literature [5, 26, 30]. The deposition rate was set to 2 mm/min with a 30 min waiting time between each dipping run to let the film air dry before the next layer deposition. A higher deposition rate (5 mm/min) was also tested, but some heterogeneous issues and empty voids were observed for the film and the use of this rate was discontinued.

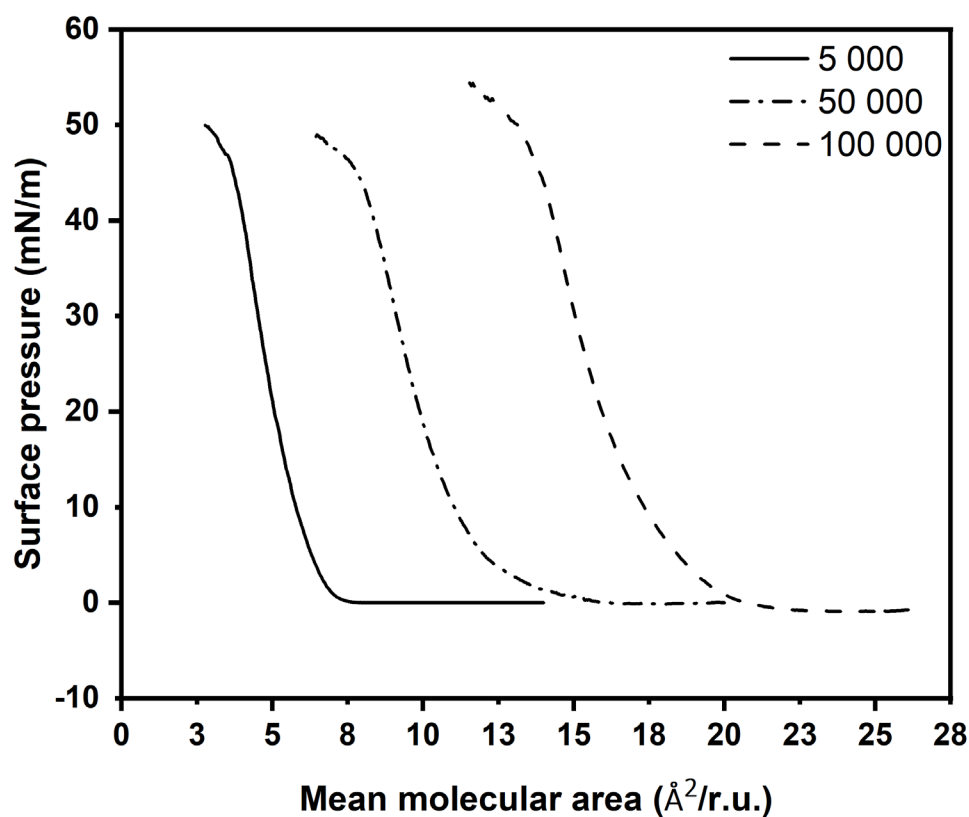


Figure 2. 2 Isotherm graph produced on the KSV-2000 instrument illustrating various phases of monolayer polyaniline film for MWs 5000, 50000, and 100000 g.mol<sup>-1</sup> and NMP + Chloroform as solvent. (Isotherm data is collected using KSV-2000 Langmuir-Blodgett Trough tool and plotted in Origin Pro 2019b.)

## 2.3 Results and Discussion

As described earlier, three different molecular weights of EB-PANi are investigated under the two dominant recipes reported in the literature to study the LB-trough PANi film properties. For film characterization, Fourier Transform Infrared (FTIR) spectroscopy was used (Thermo Scientific Nicolet iS50R FT-IR) to confirm the PANi film composition and the film doping by signature peak analysis. Atomic Force Microscopy (AFM) has been used to confirm film thickness and morphology to investigate film uniformity.

Ellipsometry (J.A. Woollam V-VASE) was used to measure film thickness and optical characteristics as a secondary measurement method.

### **2.3.1 FTIR:**

Fourier-transform Infrared (FTIR) spectroscopy is a non-destructive characterization method for identifying molecular structures, such as functional groups and bonds, qualitatively according to the characteristic frequencies data, as well as for identifying component content of the sample quantitatively according to the band intensity data. For quantitative analysis by FTIR, well-defined calibration standards are required and typically evaluated by a secondary spectroscopic techniques like nuclear magnetic resonance (NMR) [31]. Here, attenuated total reflection – Fourier transform infrared spectroscopy (ATR-FTIR) is employed in the range of  $400 - 4000 \text{ cm}^{-1}$  in the reflection mode for a qualitative analysis of the PANi LB-film formation and confirmation of the doping of the films. This measurement was repeated for both mixture preparation recipes and three molecular weights under interest (5000, 50000, and  $100000 \text{ g.mol}^{-1}$ ). However, no noticeable changes were observed in the FTIR spectra between different molecular weights for a same subphase condition. Figure 2. 3 shows the reflection FTIR spectra of 45 strokes LB-trough deposited PANi film for the three molecular weights and under two subphase conditions on a silicon substrate. To produce undoped films, deionized water subphase (Figure 2. 3 (a), (b), and (c)), and for the doped films 2-molar HCl subphase (Figure 2. 3 (d), (e), and (f)) are used in the LB-trough processing to control the protonation of the deposited film, respectively. FTIR assignment peaks for doped and undoped samples on silicon substrate are shown in Table 1.

For the undoped PANi film, absorption peaks at 2918  $\text{cm}^{-1}$  and 2848  $\text{cm}^{-1}$  are attributed to aromatic C-H stretching [21], peaks at 1585  $\text{cm}^{-1}$  and 1465  $\text{cm}^{-1}$  are ascribed to C=N and C=C stretching of the quinoid and benzenoid rings, respectively [32-34], the peak at 1273  $\text{cm}^{-1}$  is assigned to C-N stretching of the benzenoid ring [32], and the peak at 1112  $\text{cm}^{-1}$  is ascribed to the quinoid group [35]. The characteristics peaks between 1700  $\text{cm}^{-1}$  and 1100  $\text{cm}^{-1}$  wavenumbers confirm the formation of the PANi film [12, 36, 37]. The peaks presented between 2300  $\text{cm}^{-1}$  and 1800  $\text{cm}^{-1}$  are artifacts from the FTIR tool crystal and are not attributed to the PANi film.

Table 2. 1 FTIR peak assignment of 45 layers LB-trough PANi EB (5000  $\text{g}\cdot\text{mol}^{-1}$ ) for undoped and doped (2M HCl) thin films

	Peak Assignment				
LB-trough EB PANi (5000 $\text{g}\cdot\text{mol}^{-1}$ )	C-H Aromatic stretching	C=N stretching quinoid ring	C=C stretching benzenoid ring	C-N stretching benzenoid ring	Quinoid group
Undoped peak position ( $\text{cm}^{-1}$ )	2918, 2848 [21]	1585 [32-34]	1465 [32-34]	1273 [32]	1100 [36, 37]
Doped peak position ( $\text{cm}^{-1}$ )	2917, 2848 [21]	1588 [21, 38]	1469 [21, 38]	1280 [21, 38]	1116 [21, 38]

In each Emeraldine Base PANi unit there are two benzenoid amines (-NH-) and two quinoid imines (=N-) (Figure 2. 1), where the latter two are subject to be protonated in acidic solutions [39] which is HCl in this case. In the doping mechanism of EB-PANi, the iminic nitrogen atoms (C=N) can be protonated in whole or partial to perform the

corresponding salts. The degree of protonation “doping” depends on the pH level of the aqueous dopant acid [40]. The protonated polymer, “(EBH)<sup>+</sup>Cl<sup>-</sup>,” is a stable delocalized polysemiquinone radical cation which has a half filled polaron conduction band and is a key factor in electrically conductive polyaniline [40].

For the HCl-doped protonated PANi film, characteristic peaks between 1700 cm<sup>-1</sup> and 1100 cm<sup>-1</sup> are blue-shifted and show an increase in relative intensities. These changes are previously reported on HCl doped LB-PANi film and are attributed to the confirmation of the doping [21, 38]. The blue shifts are ascribed to radical cations and an increase in actual conjugation length in the polymer chain [38]. The increase in relative intensities of the absorption bands, on the other hand, is attributed to increasing in the molecular dipole moments of the polymer due to the protonation of the amine and imine units [21].

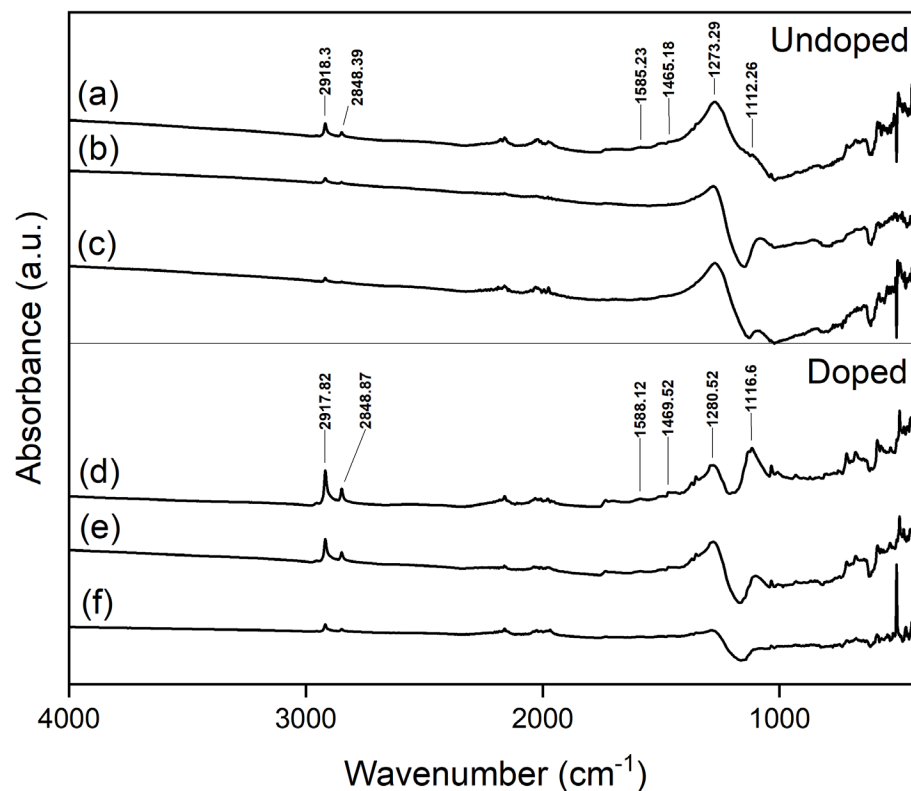


Figure 2. 3 Reflectance ATR-FTIR spectra of LB-PANi films for undoped (DI water subphase) at top and doped (2M HCL subphase) at the bottom, (a) 5000 g.mol<sup>-1</sup>, (b) 50000 g.mol<sup>-1</sup>, (c) 100000 g.mol<sup>-1</sup>, (d) 5000 g.mol<sup>-1</sup>, (e) 50000 g.mol<sup>-1</sup>, (f) 100000 g.mol<sup>-1</sup>. (Data is collected using Thermo Scientific Nicolet iS50R FT-IR and plotted in Origin Pro 2019b.)

### 2.3.2 Transfer ratio analysis

A successful deposition using the LB-trough technique depends on the formation and stability of monolayers on top of the subphase. The surface tension of water is 73 mN/m at 20 °C in ambient pressure. This is a remarkably high value compared to most other liquids and a primary reason to consider using it for polymer thin film deposition in general and specifically for PANi LB-trough deposition. Manigandan, et al. shown that the type of the solvent and mixture preparation can change the PANi chain nanostructure from a spiral to

a more nanorod conformation, changing the physical and electrical properties of the LB-trough PANi film as well [41]. The nanostructure configuration of the PANi chain is beyond the scope of this paper, but in this regard, the study of molecular weight impacts on PANi films followed the two most commonly utilized process solutions for preparing the polyaniline for LB-trough processing and may speak to this impact [20, 26].

The main goals of this research were to study the impacts of the two polyaniline mixture preparation recipes under investigation for LB-trough deposition, the impact of the EB-PANi polymer molecular weights on the process, and the impact of the subphase acidity state on the deposition characteristics and film quality. In this regard, the transfer ratio of the depositions was explored (Figure 2. 4). The transfer ratio is described as the ratio between the decrease in monolayer area on top of the subphase during a deposition stroke (immersion or withdrawal), and the area of the substrate. This value can provide information about the quality and the type of the deposition. For an ideal transfer, the transfer ratio is equal to 1. There are three different deposition types for LB-trough films: X-type deposition usually happens on a hydrophobic surface, and amphiphilic molecules are deposited in head-to-tail order only when the substrate is dipping down into the subphase (immersion); Y-type deposition occurs on a hydrophilic surface and in both up (withdrawal) and down directions (immersion). This will result in tail-to-tail and head-to-head orientations for amphiphilic molecules; Z-type deposition typically needs a hydrophilic surface, and the deposition happens only in the upward direction (withdrawal). Molecules deposited by Z-type deposition have tail-to-head orientation on a multilayer stack of the resulting LB film.

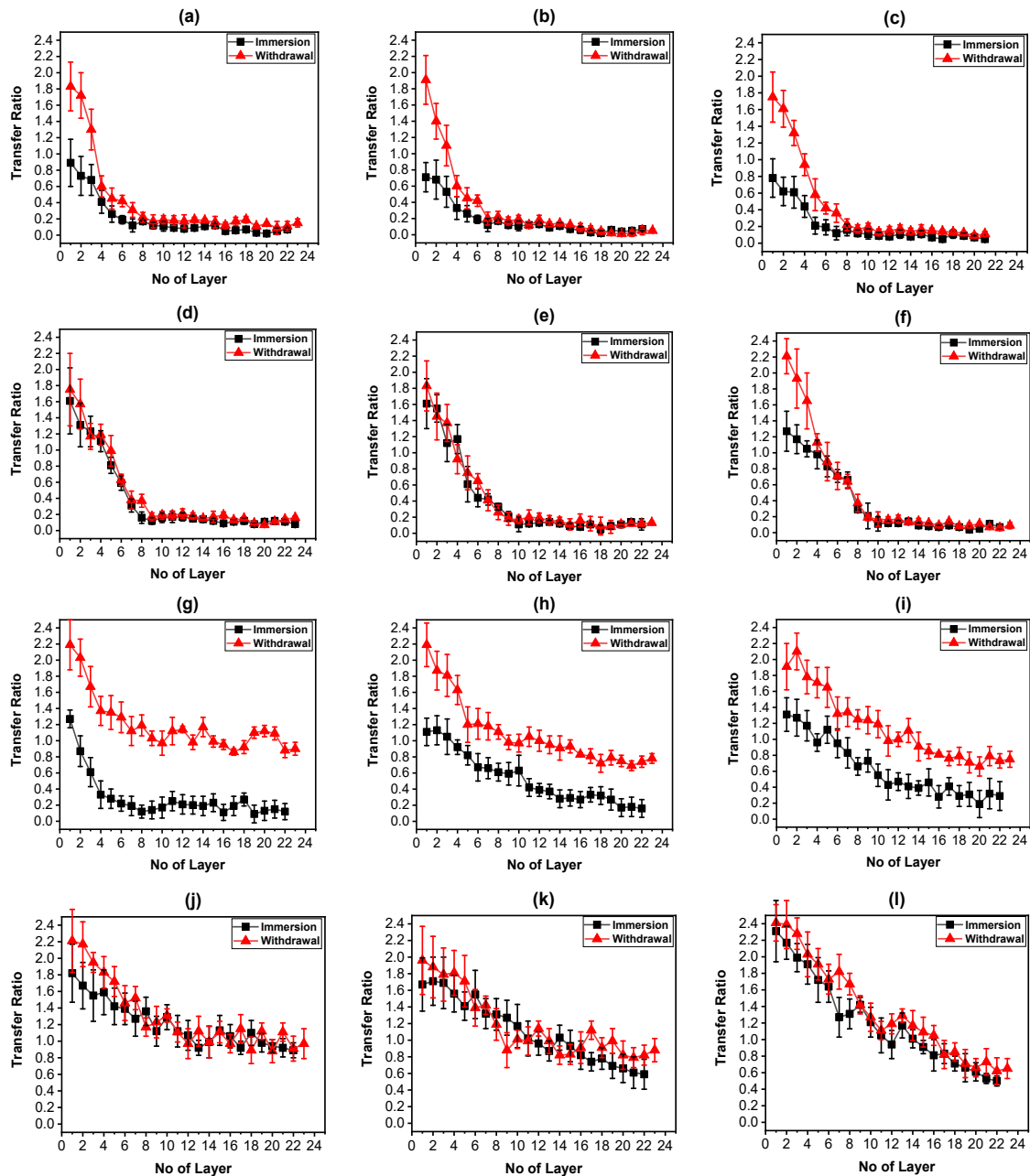


Figure 2. 4 The transfer ratio of 45 strokes LB-trough EB PANi film for three molecular weights, two different recipes (NMP only and NMP+Chloroform as solvent) and two different subphase (DIW and 2M HCl) on silicon substrate. (a) MW 5000 g.mol<sup>-1</sup>, NMP solvent, DIW subphase. (b) MW 50000 g.mol<sup>-1</sup>, NMP solvent, DIW subphase. (c) MW 100000 g.mol<sup>-1</sup>, NMP solvent, DIW subphase. (d) MW 5000 g.mol<sup>-1</sup>, NMP solvent, 2M HCl subphase. (e) MW 50000 g.mol<sup>-1</sup>, NMP solvent, 2M HCl subphase. (f) MW 100000 g.mol<sup>-1</sup>, NMP solvent, 2M HCl. (g) MW 5000 g.mol<sup>-1</sup>, NMP+Chloroform solvent, DIW subphase. (h) MW 50000 g.mol<sup>-1</sup>, NMP+Chloroform Solvent, DIW subphase. (i) MW 100000 g.mol<sup>-1</sup>, NMP+Chloroform Solvent, DIW subphase. (j) MW 5000

g.mol<sup>-1</sup>, NMP+Chloroform Solvent, 2M HCl subphase. (k) MW 50000 g.mol<sup>-1</sup>, NMP+Chloroform solvent, 2M HCl subphase. (l) MW 100000 g.mol<sup>-1</sup>, NMP+Chloroform solvent, 2M HCl subphase. (Transfer ratio data is collected using KSV-2000 Langmuir-Blodgett Trough tool and plotted in Origin Pro 2019b.)

The transfer ratio graphs, Figures 2. 4a to 4f show that the mixture preparation recipe using NMP only as the solvent, gives successful deposition only for a few layers (number of layers  $\leq 5$ ). The results indicate that the top layer will lose its hydrophilic properties for thicker films, which is a critical parameter for successful PANi LB-trough film deposition. To confirm this hypothesis, atomic force microscopy was used to qualify the film's uniformity (supplemental material Figure S.2). The AFM images showed non homogenous properties for the film with grain boundaries ranging from 1 and 3  $\mu\text{m}$  in size with empty voids between them. It also reveals that deposition type is Z-type for DIW subphase when deposition takes place only on withdrawal strokes, shown in Figures 2. 4a to 4c and is a Y-type deposition for acidic (2M HCl) subphase when deposition takes place in both immersions and withdrawals, shown in Figures 2. 4d to 4f.

However, the recipe using NMP + chloroform as the solvent demonstrated a higher rate of deposition success, shown in Figures 2. 4g to 4l. The PANi film preserved its hydrophilic properties through 45 layers of deposition without indication of any limitation in the process if additional thickness is required for the application. The deposition type again is a Z-type for neutral DIW subphase, shown in Figures 2. 4g to 4i, and a Y-type deposition for the acidic (2M HCl) subphase, shown in Figures 2. 4j to 4l. The Y-type deposition

might be explained by forming of polarons in results of iminic nitrogen atoms protonation in the PANi polymer chain and increasing the van der Waals forces between the LB-Trough PANi film layers. Further investigation is needed to confirm this hypothesis.

Comparing the transfer ratio of the three characterized EB-PANi molecular weights (MWs), no significant change was observed for the recipe with NMP only as the solvent. Using this recipe regardless of the molecular weight of the polymer chain, the deposition proceeded to a few layers and resulted in a non-uniform film deposition on the oxidized silicon substrate. However, the transfer ratio graphs for the NMP + Chloroform, Figures 2. 4g to 4l demonstrated that the 5000 g.mol<sup>-1</sup> MW produced the best film properties in uniformity and in a consistent deposition process (Figure 2. 4g). This result can be correlated to the PANi chain length and its amphiphilic properties on the water surface. Simply stated, it is more difficult for heavier PANi chains to suitably float properly oriented on the water surface than lighter ones. This means a lower molecular weight PANi chain can produce a more consistently uniform film more readily than for longer and heavier PANi molecular chains. Considering the transfer ratio graphs, no significant difference in result was observed between the two heavier MWs (50000 and 100000 g.mol<sup>-1</sup>). Both MWs started the process with a transfer ratio above two (>2), which dropped to below 1 after 20 strokes. However, the 5000 g.mol<sup>-1</sup> transfer ratio stabilized around 1 after 10 strokes and remained at that same ratio through 45 process strokes.

At this point, the recipe using NMP + chloroform as the solvent and the 5000 g.mol<sup>-1</sup> MW PANi was chosen as the most promising process candidate for LB-PANi film quality from a commercially-available initial emeraldine base source material.

### **2.3.3 AFM:**

To measure the LB-trough PANi film's thickness and surface roughness, a Bruker Dimension ICON AFM has been used in tapping mode, 0.5 Hz scan rate, and 256 samples per line. For each sample, four different scan sizes were produced: 9, 3, 1, and 0.5  $\mu\text{m}^2$ . Figure 2. 5 gives a representative sample of the measurements taken for an undoped 45 layer 5000 g.mol<sup>-1</sup> PANi film for the NMP+chloroform recipe sample. In atomic force microscopy, height sensor data is useful to collect accurate topographical information. The position of the piezo during the scan reflects the height of the sample. The amplitude error data which is collected with a high feedback gain and simultaneously with the height data (the case here), essentially equals the derivative of the height sensor data. Although, amplitude error data alone does not provide quantitative information, it can be used in visualizing fine details in topography that are difficult to see in regular height data [42] (Figure 2. 5). For the surface roughness analysis, the first order of flattening and the plane fit was conducted on height sensor image before collecting the data. Surface roughness was calculated by the root-mean-square (RMS) average of height deviations taken from the mean image data plane. For the film thickness, a step measurement method was used (Figure 2. 6). In the step analysis, relative height measurements between two regions on sample surfaces are compared. Here, because there are no features on the samples, a sharp blade was used to make a step edge on PANi film. Again, Figure 2. 6 gives a representative

sample of the measurements taken for the undoped 45 strokes 5000 ( $\text{g}\cdot\text{mol}^{-1}$ ) PANi film for the NMP + chloroform recipe sample.

To examine the multilayer behavior of the LB-trough PANi film, two different thicknesses (15 and 45 strokes) were studied under two different subphase conditions, neutral deionized water for an undoped film and an acidic subphase (2 molar HCl) for the doped film. These examination studies were repeated for all three PANi-EB molecular weights (5000, 50000, and 100000  $\text{g}\cdot\text{mol}^{-1}$ ) and for both recipes utilized in the study. The AFM thickness and surface roughness data analysis are provided further in this section (Figure 2. 8). All the detailed data are provided as supplemental material in Table S.1.

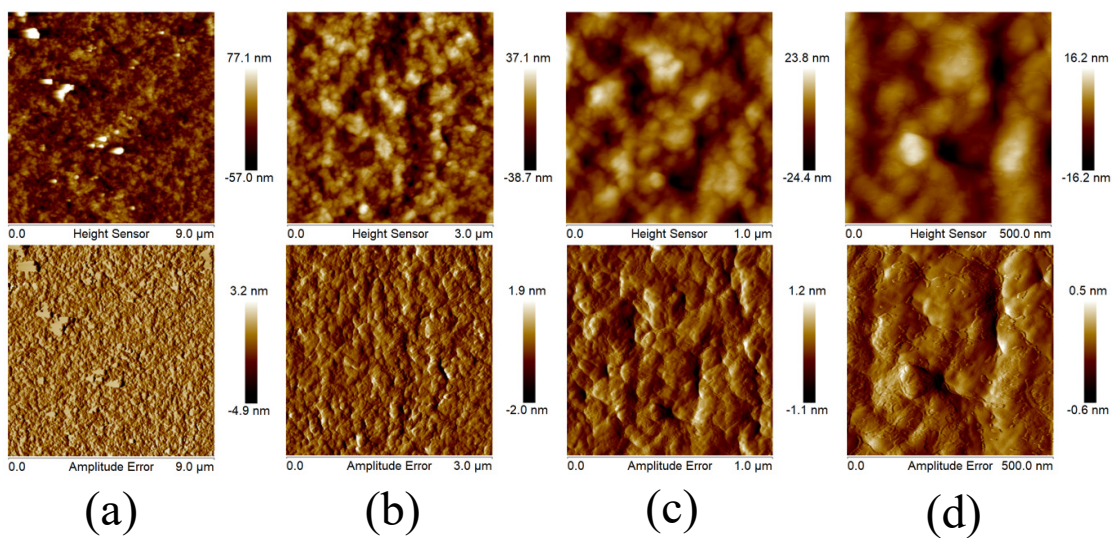


Figure 2. 5 AFM images of LB-trough PANi film, 45 strokes, molecular weight = 5000  $\text{g}\cdot\text{mol}^{-1}$ , doped, NMP + chloroform solvent. Top row images are height sensor and bottom row images are amplitude error images for different scan sizes (a) 9  $\mu\text{m}$ , (b) 3  $\mu\text{m}$ , (c) 1  $\mu\text{m}$ , (d) 500 nm (data collected by Bruker Dimension ICON AFM).

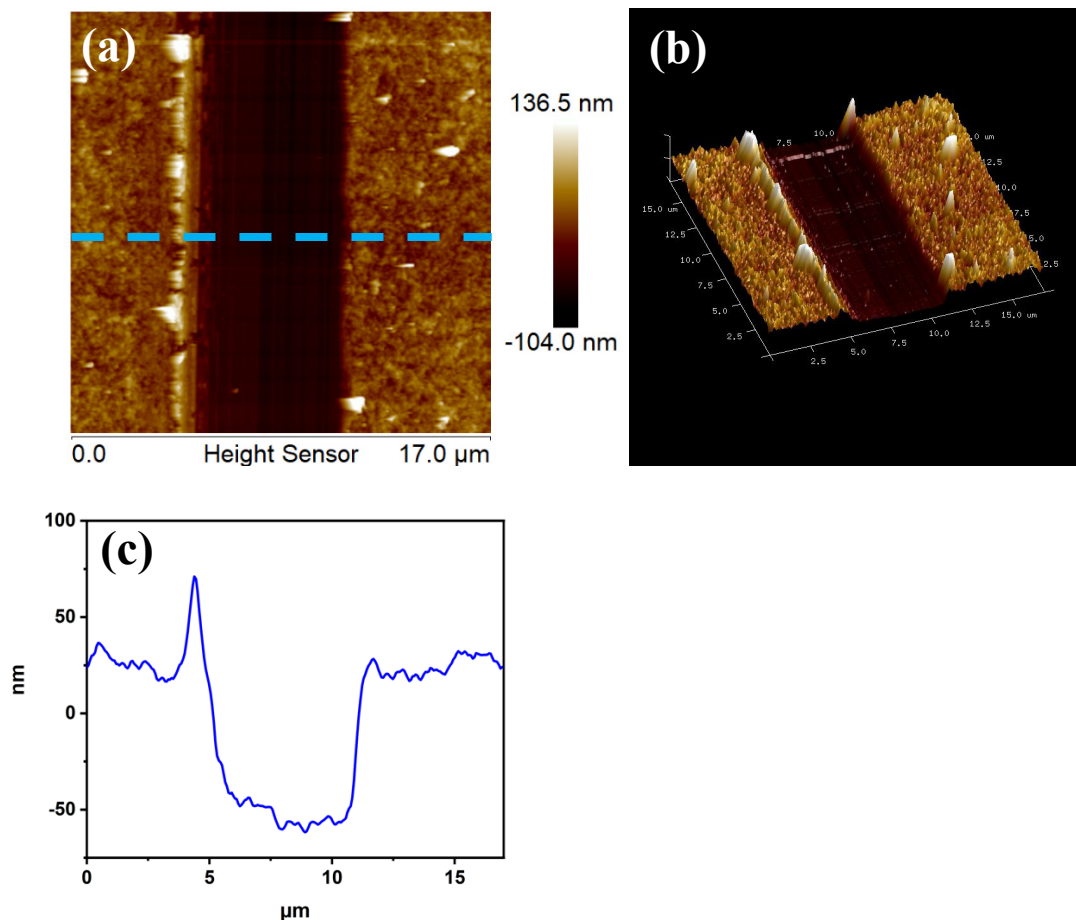


Figure 2. 6 AFM images of the  $5000 \text{ g.mol}^{-1}$  LB-trough PANi film for the thickness measurement. (a) 2-dimensional image with a scan size of  $17 \mu\text{m}$ . A step edge was made in the film using a sharp blade. (b) 3-dimensional perspective image. (c) Cross-section profile across the indicated dashed line in (a). (data collected by Bruker Dimension ICON AFM).

### 2.3.4 Spectroscopic Ellipsometry:

Spectroscopic ellipsometry is a highly sensitive and non-destructive characterization method that measures polarization changes in reflected or transmitted light over wavelength from a sample to determine the thickness and/or optical properties of a material [43]. In this study, spectroscopic ellipsometry is used to measure the PANi film thickness

as a secondary measurement method to support and confirm the AFM results. Because ellipsometry utilizes optical model parameters to fit the data, it is necessary to have sufficient data from the sample, including the material, layer structure and thickness range for each layer, optical properties (transparent, absorbing), crystallinity, and surface roughness. The model fit using the ellipsometry measurement is improved when more characteristics are known about the sample parameters .

In all measurements here, a J.A. Woollam V-VASE spectroscopic ellipsometer was used over the wavelength range of 300 – 1500 nm, and at three different incident angles of 65°, 70°, and 75°. The PANi film thickness measurement was performed in two steps. First, the substrate's silicon oxide (SiO<sub>2</sub>) layer thickness was measured prior to PANi deposition, and then a second measurement was performed after PANi deposition. The CAUCHY function was utilized as the model fit for the PANi film thickness measurement given the prior characterization of the silicon oxide thickness from the first step on the silicon substrate. The CAUCHY function has been utilized previously for polymers model fits in prior studies [44, 45]. The ellipsometry measurement and fitting data for two different locations on a 45 layer undoped PANi film is shown in Figure 2. 7 as a representative example of the measurements taken in this study.

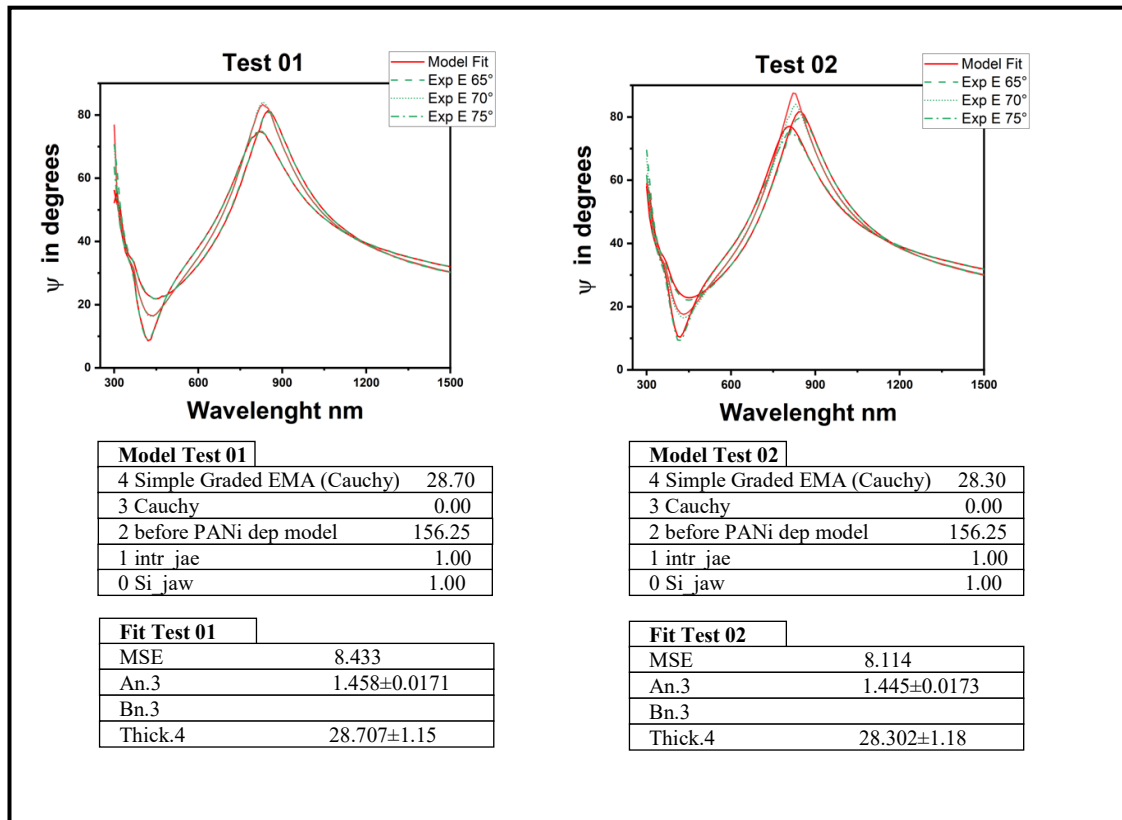


Figure 2. 7 Measurement and fitting graph for the wavelength range 300 – 1500 nm, the sample model and fitting parameters with relative error for two different spots on the sample (data is collected by J.A. Woollam V-VASE ellipsometry and plotted in Origin Pro 2019b).

In the fitting model, layer # 0 (si\_jaw) is defined as the substrate, which is lightly doped single crystal (100) silicon. In the ellipsometry modeling software (WVASE), the substrate thickness is assumed to be infinite and entered 1 mm as a default value. Layer #1 (intr\_jaw) is the native oxide interface layer between the substrate and the thermal growth oxide layer. Adding the interface layer will help to achieve a better model fit. Layer #2 (before PANi dep model) is the thermally grown silicon oxide layer and measured in the first step before the film deposition. Occasionally the optical constant of a layer is not a constant number throughout the layer. This can be because of the process variations during the film deposition. By adding graded properties to the model, the layer is divided into sublayers

with small thicknesses, and each sub-layer has slightly different optical properties [46]. Layer #3 (Cauchy) is the PANi film, and layer #4 (simple graded EMA Cauchy) is employed to add graded properties to PANi film because of having a layer-by-layer structure due to the deposition method. Again, adding graded properties to PANi film results in a more accurate fitting model.

The equation 1 defines the CAUCHY function. As is shown, it has three parameters to fit ( $A_n$ ,  $B_n$ , and  $C_n$ ), but mostly  $A_n$  and  $B_n$  are used in data fitting, and  $C_n$  is only used when it improves the mean square error (MSE) 10% or more. In ellipsometry data fitting, it is recommended to fit as few parameters as possible to avoid correlation between parameters and reduce the fitting complexity [46]. The index is modeled as

$$n(\lambda) = A_n + \frac{B_n}{\lambda^2} + \frac{C_n}{\lambda^4} \quad \text{Equation 1}$$

where  $\lambda$  is the wavelength,  $A_n$  relates to the approximate amplitude for the material index, while  $B_n$  and  $C_n$  parameters provide the shape or curvature of the index versus wavelength [46]. The AFM step edge measurement for the same sample showed 24.6 nm, which is in close agreement with the ellipsometry measurement. (More details of Cauchy parameterization is available as supplemental material Figure S.1).

### 2.3.5 Thickness and surface roughness analysis

To examine the film deposition's reproducibility, five samples of the  $5000 \text{ g.mol}^{-1}$  MW LB-PANi films each were investigated for 15- and 45-layer thicknesses for both doped (2-molar HCl subphase) and undoped (DIW subphase) depositions. The film thickness and uniformity results are shown in Figure 2. 8. The raw data, including all relevant details, are provided in supplemental material Table S.1.

Figure 2. 8a summarizes the film thickness study. The average film thickness for undoped 15 strokes is 16 nm. Since it is a Z-type deposition, there are 8 layers of PANi film deposited during upward direction and an average thickness of 2 nm/layer. For the undoped 45 strokes the single layer film thickness drops to 1.1 nm/layer. This monolayer film thickness variation between 15 and 45 strokes can be explained by transfer ratio graph (Figure 2. 4g) that shows deposition occurs in both immersion and withdrawal directions for the first few strokes before it reaches to steady state. The average film thickness for doped 15 and 45 strokes are 22.9 nm and 98.2 nm respectively. Because it is a Y-type deposition, shown in transfer ratio graph (Figure 2. 4j), the single layer film thickness for doped 15 and 45 strokes will be 1.5 and 2.2 nm/layer respectively. In result, a LB-Trough deposited PANi monolayer film thickness for  $5000 \text{ g.mol}^{-1}$  is between 1.1 and 2.2 nm which is in agreement with the literature [6, 47].

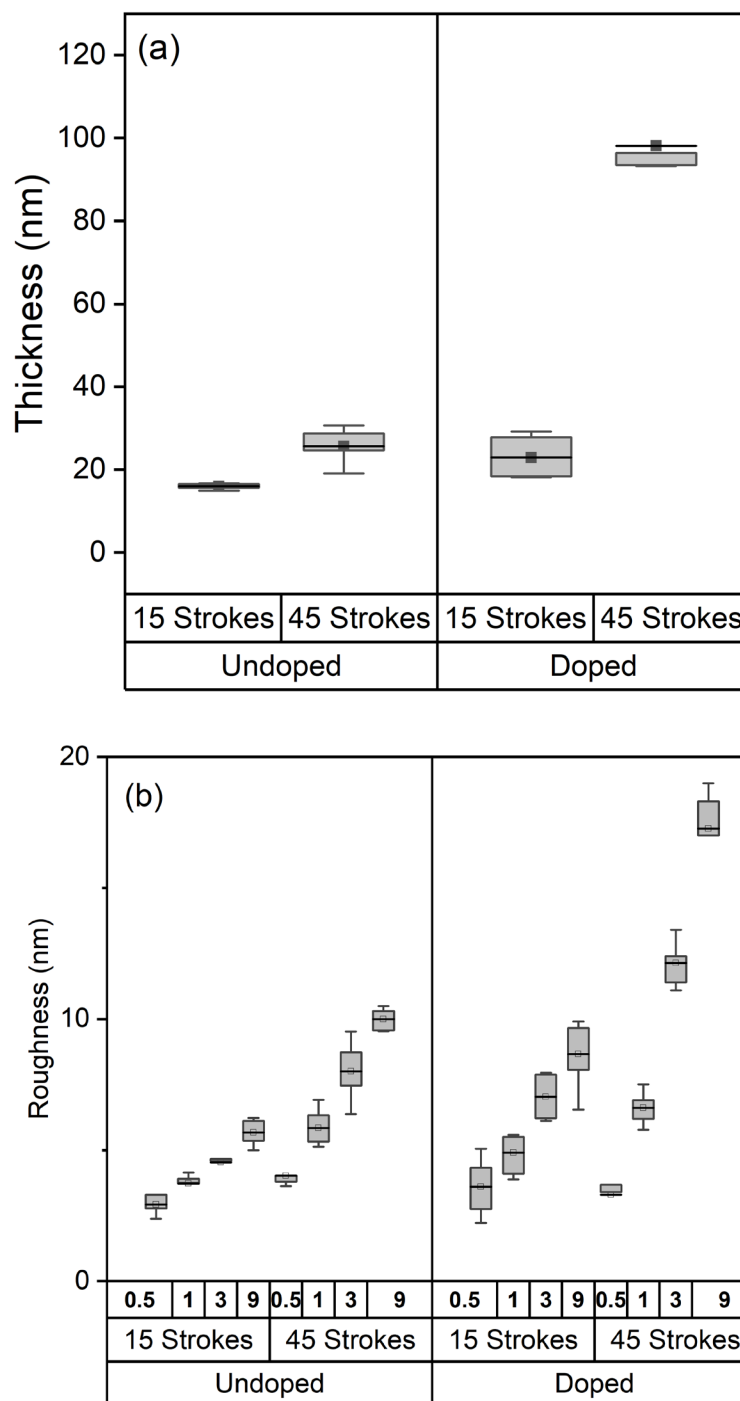


Figure 2. 8 LB-trough PANi 5000 g.mol<sup>-1</sup> MW film thickness and roughness AFM measurement according to number of layers and doping state: (a) AFM film thickness measurement (b) Root Mean Square (RMS) roughness AFM data for various area sizes 0.5, 1, 3, and 9  $\mu\text{m}^2$ . (Data is collected by Keithley 4200A-SCS parameter analyzer and plotted in Origin Pro 2019b).

Figure 2. 8b shows RMS roughness data of four scanned area sizes (0.5, 1, 3, and 9  $\mu\text{m}^2$ ) for 15 and 45 strokes LB-Trough PANi films deposited on silicon substrates under two subphase statuses. The graph shows that average RMS roughness increases by increasing the scanning area i.e., 0.5  $\mu\text{m}^2$  scanned area has a smoother surface compared to 9  $\mu\text{m}^2$  in all groups. The RMS roughness also climbs by increasing the film thickness under the same doping status. For example, doped 15 strokes average RMS roughness is 6 nm while doped 45 strokes mean is 10 nm and this is also through for undoped films. Another significant outcome of this graph is that doped films have higher RMS roughness level versus undoped films for the same number of strokes. For instance, 45 strokes doped film average RMS roughness is 10 nm while it is 7 nm for 45 strokes undoped films. The reason can be explained by the fact that doped films are thicker compared to undoped films for a same number of strokes because of having a Y-type deposition versus Z-Type respectively.

### **2.3.6 Electrical characterization**

The DC conductivity of polyaniline LB-Trough films have been reported previously [7, 48]. Depending on the oxidation state and the protonation level, the conductivity can vary from  $10^{-12}$  S.cm<sup>-1</sup> (Emeraldine base) to  $10^{-2}$  S.cm<sup>-1</sup> (Emeraldine salt) [11]. Interdigitated electrode contacts have been used here for the DC conductivity measurement at room temperature using the same method reported in the past [2, 48]. Figure 2. 9a shows the current-voltage data for 45 strokes deposited 5000 g.mol<sup>-1</sup> LB-Trough PANi film. Acidic subphases (HCl) with various molarity levels were used for the PANi film protonation. The highest conductivity achieved by the commercial PANi was  $10^{-9}$  S.cm<sup>-1</sup>, which is significantly below the previously reported data [11]. The FTIR absorption spectra with

the acidic subphase produced the expected blue shift in peaks indicating protonation, and contrasting the experimental electrical measurements. Multiple changes in the process and the source chemicals were explored to seek to improve the conductivity such as: using interdigitated electrodes with different spacings (1, 2, 5, and 10  $\mu\text{m}$ ), and purchasing new commercial PANi source materials and solvents to eliminate any impact of materials' potential shelf-life degradation. However, no noticeable enhancement in the measurement was observed. For comparison, an oxidative synthesis polymerization method that has been reported previously [24] was processed to produce a comparative film to replace the commercial emeraldine PANi source material while keeping all other conditions of the process and materials the same. Based on the data reported by Mattoso et al. [24], the synthesis reaction temperature was kept around 5  $^{\circ}\text{C}$  to reproduce EB-PANi with molecular weight close to 5 000  $\text{g}\cdot\text{mol}^{-1}$ . The results showed 8 orders of magnitude improvement in conductivity. The current-voltage data of samples using the synthesized PANi are shown in Figure 2. 9b. The highest conductivity that was achieved with the synthesized PANi was 0.1  $\text{Scm}^{-1}$ , which is comparable with reported data in the literature [47]. The reason that commercial 5000  $\text{g}\cdot\text{mol}^{-1}$  PANi films have a low conductivity in this study is unclear, but may have a root cause in the polymerization method and/or the oxidative state of the polymer as delivered; however, the commercial processes and methods remain proprietary and unavailable for detailed consideration in this study. Further investigation is needed to explore the primary mechanisms why commercial LB-Trough deposited EB PANi has very low conductivity while exhibiting FTIR, AFM, spectroscopic ellipsometry, and film thickness and process parameters that align with the synthesized material.

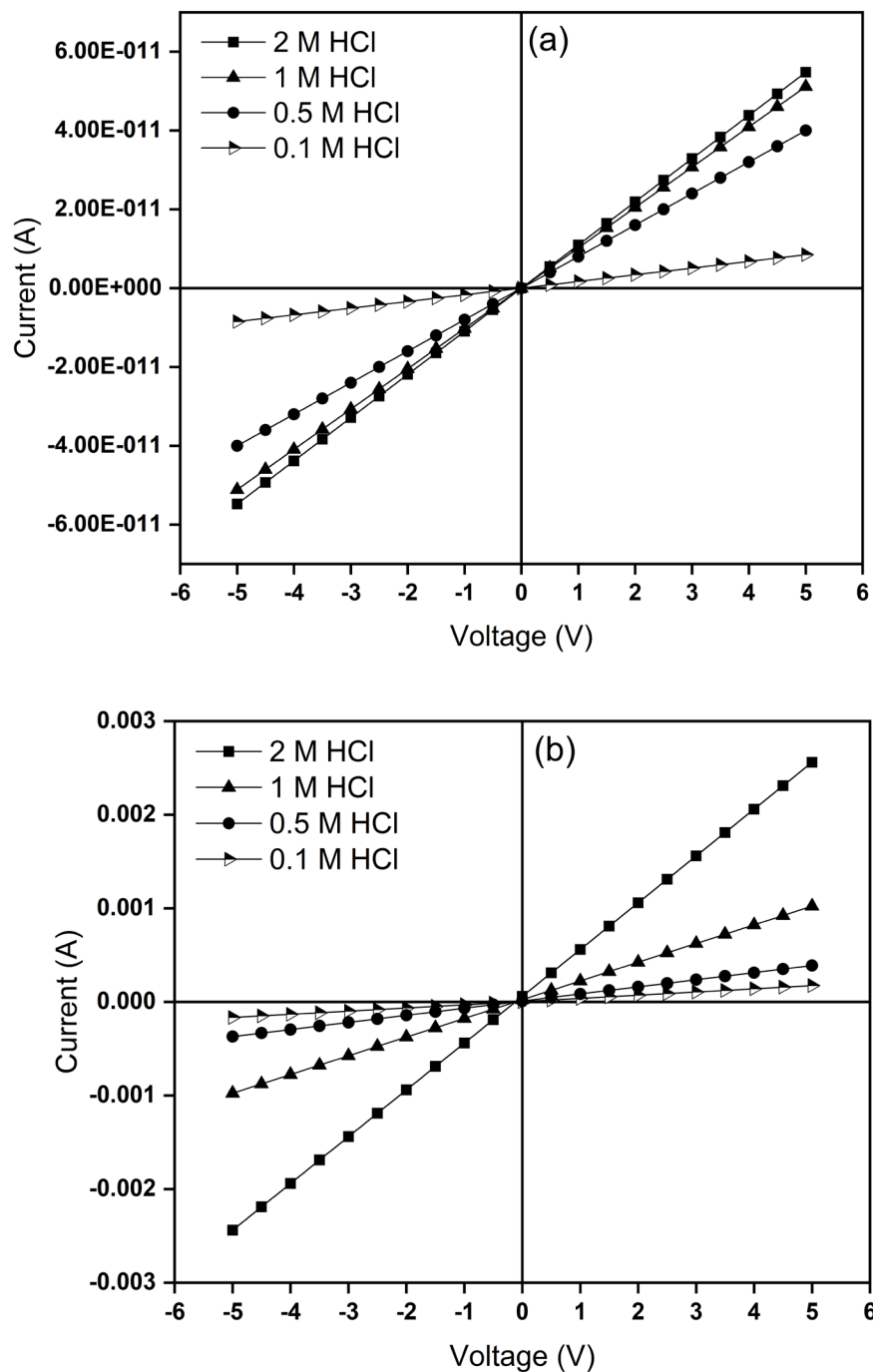


Figure 2. 9 Current–voltage graph with different levels of doping for 45 strokes LB-Trough deposited PANi films on interdigitated electrodes: (a) commercial 5000 g.mol<sup>-1</sup> emeraldine PANi, (b) oxidative synthesized emeraldine PANi (Data is collected by Keithley 4200A-SCS parameter analyzer with measurement resolution of  $\pm 0.2 \mu\text{V}$ ,  $\pm 100 \text{ fA}$  and plotted in Origin Pro 2019b).

## 2.4 Conclusions

The LB-trough EB-PANi film deposition was evaluated for two different mixture preparation recipes, three molecular weights (5000, 50000, and 100000 g.mol<sup>-1</sup>), and under two different subphase conditions (neutral DIW and 2M HCl). The FTIR absorption spectra peaks assignment revealed PANi thin film formation and a blue shift of the PANi signature peaks between 1700 cm<sup>-1</sup> and 1100 cm<sup>-1</sup> confirming film doping under the 2M HCl subphase conditions. Spectroscopic ellipsometry was used to characterize the LB-trough PANi film thickness measurement employing a graded Cauchy model. By monitoring the LB-trough thin film deposition transfer ratio and film thickness measurements using AFM and ellipsometry, the study confirmed Z-type deposition for undoped (DIW subphase) and Y-type deposition for doped (2M HCl subphase) LB-trough EB-PANi film. A further study is required to fully understand this mechanism and also investigate if there is any similar behavior for any other LB-Trough deposited film. The recipe with NMP only as the solvent, showed successful deposition for only a few layers ( $\leq 5$ ) and considerable nonuniformity issues in the deposited films. The impact of the NMP solvent only on the EB-PANi polymer chain under deposition conditions remains unclear and warrants further investigation. Demonstrated reproducibility of the mixture with NMP + Chloroform as solvents with a source PANi molecular weight of 5000 g.mol<sup>-1</sup> is presented as a promising thin film deposition condition in terms of film quality, excellent thickness control with 1.1 – 2.2 nm/layer depending on subphase conditions while producing a uniform and homogenous film. Thin film surface roughness measurements revealed a smoother film by a factor of two for an undoped versus a doped film. The commercial 5000 g.mol<sup>-1</sup> EB-PANI exhibited very low conductivity in DC electrical measurements compared to the

synthesized films, and future work is needed to reveal the primary mechanisms. High conductivity  $0.1 \text{ S.cm}^{-1}$  LB-trough-based PANi film deposition can be achieved by employing the oxidative synthesized polymerization method for the EB-PANi source material in mixture preparation.

## **2.5 Acknowledgements**

This work was supported by funding from Michigan Technological University, through the College of Engineering and the Department of Electrical and Computer Engineering. The authors gratefully acknowledge support from Dr. Kathryn Perrine, Department of Chemistry, in the FTIR study and analysis of PANi films, from the Advanced Chemical and Morphological Analysis Laboratory in the AFM analysis, and from Dr. Chito Kendrick and Dr. Andrew J. Gross, Microfabrication Facility, Department of Electrical and Computer Engineering, for support in the processing and other characterization capabilities utilized in this study, all at Michigan Technological University.

## 2.6 References

1. T. M. Daunais and P. L. Bergstrom, “Silicon nanowire-based biosensors for low concentration detection of *salmonella* and *escherichia coli* in complex mixtures,” *Proc. IEEE 13th Nano Materials and Devices Conference (NMDC 2018)*, 13–17 October 2018, Portland, OR, 21–24.
2. Agbor, N., M. Petty, and A. Monkman, *Polyaniline thin films for gas sensing*. Sensors and Actuators B: Chemical, 1995. **28**(3): p. 173-179.
3. Farag, A., A. Ashery, and M.A. Rafea, *Optical dispersion and electronic transition characterizations of spin coated polyaniline thin films*. Synthetic metals, 2010. **160**(1-2): p. 156-161.
4. Rozemarie, M., et al. *Electrospun Based Polyaniline Sensors—A Review*. in *IOP Conference Series: Materials Science and Engineering*. 2017. IOP Publishing **209** 012063
5. Prabhakar, N., Z. Matharu, and B. Malhotra, *Polyaniline Langmuir–Blodgett film based aptasensor for ochratoxin A detection*. Biosensors and Bioelectronics, 2011. **26**(10): p. 4006-4011.
6. Zhang, T., et al., *Engineering crystalline quasi-two-dimensional polyaniline thin film with enhanced electrical and chemiresistive sensing performances*. Nature communications, 2019. **10**(1): p. 1-9.
7. Özbek, Z., F. Davis, and R. Capan, *Electrical properties of alternating acid and amino substituted calixarene Langmuir-Blodgett thin films*. Journal of Physics and Chemistry of Solids, 2020. **136**: p. 109146.

8. de Souza, N.C., et al., *Morphological characterization of Langmuir–Blodgett films from polyaniline and a ruthenium complex (Rupy): influence of the relative concentration of Rupy*. *Nanotechnology*, 2007. **18**(7): p. 075713.
9. Michira, I., et al. *Synthesis, characterisation of novel polyaniline nanomaterials and application in amperometric biosensors*. in *Macromolecular symposia*. 2007. Wiley Online Library. Pages 57-69 <https://doi.org/10.1002/masy.200750907>
10. Masters, J., et al., *Polyaniline: allowed oxidation states*. *Synthetic Metals*, 1991. **41**(1-2): p. 715-718.
11. Rajapakse, R., A.C. Perera, and H. Premasiri, *Polyaniline retained glass templates as sensors for acidic/basic and/or redox gases*. *Journal of the National Science Foundation of Sri Lanka*, 2010. **28**(4). P. 277-285
12. Bhullar, G.K., R. Kaur, and K. Raina, *Hybrid polyaniline–TiO<sub>2</sub> nanocomposite Langmuir–Blodgett thin films: Self-assembly and their characterization*. *Journal of Applied Polymer Science*, 2015. **132**(5). <https://doi.org/10.1002/app.41386>
13. Gurunathan, K. and D.C. Trivedi, *Studies on polyaniline and colloidal TiO<sub>2</sub> composites*. *Materials Letters*, 2000. **45**(5): p. 262-268.
14. Noriega, R., et al., *A general relationship between disorder, aggregation and charge transport in conjugated polymers*. *Nature materials*, 2013. **12**(11): p. 1038-1044.
15. Lee, H.-J., et al., *Close-packed polymer crystals from two-monomer-connected precursors*. *Nature communications*, 2016. **7**(1): p. 1-6.

16. Xie, D., et al., *Fabrication and characterization of polyaniline-based gas sensor by ultra-thin film technology*. Sensors and Actuators B: Chemical, 2002. **81**(2-3): p. 158-164.
17. Chen, C.-W., J.-H. Yeh, and T.-J.J.T.S.F. Liu, *Stable Langmuir–Blodgett film deposition of polyaniline and arachidic acid*. 2007. **515**(18): p. 7299-7306.
18. Goldenberg, L., M. Petty, and A. Monkman, *A Comparative Study of the Electrochemical Properties of Dip-Coated, Spun, and Langmuir-Blodgett Films of Polyaniline*. Journal of the Electrochemical Society, 1994. **141**(6): p. 1573-1576.
19. Riul Jr, A., et al., *Characterization of Langmuir-Blodgett films of parent polyaniline*. Thin Solid Films, 1996. **284**: p. 177-180.
20. Dhanabalan, A., et al., *A Study of Langmuir and Langmuir– Blodgett Films of Polyaniline*. Langmuir, 1997. **13**(16): p. 4395-4400.
21. Cheung, J. and M. Rubner, *Fabrication of electrically conductive Langmuir-Blodgett multilayer films of polyaniline*. Thin Solid Films, 1994. **244**(1-2): p. 990-994.
22. Ram, M., N. Sundaresan, and B. Malhotra, *Langmuir-Blodgett films of processable polyaniline*. The Journal of Physical Chemistry, 1993. **97**(45): p. 11580-11582.
23. Ćirić-Marjanović, G., *Recent advances in polyaniline research: Polymerization mechanisms, structural aspects, properties and applications*. Synthetic metals, 2013. **177**: p. 1-47.
24. Mattoso, L.H., A.G. MacDiarmid, and A.J. Epstein, *Controlled synthesis of high molecular weight polyaniline and poly (o-methoxyaniline)*. Synthetic Metals, 1994. **68**(1): p. 1-11.

25. Dabke, R., et al., *Electrochemistry of polyaniline Langmuir–Blodgett films*. Thin Solid Films, 1998. **335**(1-2): p. 203-208.
26. Agbor, N., et al., *Langmuir-Blodgett films of polyaniline*. Synthetic metals, 1993. **57**(1): p. 3789-3794.
27. Kern, W., *Handbook of semiconductor wafer cleaning technology*. New Jersey: Noyes Publication, 1993: p. 111-196.
28. Paddeu, S., M.K. Ram, and C. Nicolini, *Investigation of ultrathin films of processable poly (o-anisidine) conducting polymer obtained by the Langmuir–Blodgett technique*. The Journal of Physical Chemistry B, 1997. **101**(24): p. 4759-4766.
29. Granholm, P., J. Paloheimo, and H. Stubb, *Langmuir-Blodgett films of polyaniline: Fabrication and transport studies*. Physical Review B, 1997. **55**(20): p. 13658.
30. Chen, C.-W., J.-H. Yeh, and T.-J. Liu, *Stable Langmuir–Blodgett film deposition of polyaniline and arachidic acid*. Thin Solid Films, 2007. **515**(18): p. 7299-7306.
31. Stuart, B., *Infrared spectroscopy*. Kirk-Othmer encyclopedia of chemical technology, 2000. <https://doi.org/10.1021/j150469a016>
32. Adhikari, S. and P. Banerji, *Enhanced conductivity in iodine doped polyaniline thin film formed by thermal evaporation*. Thin Solid Films, 2010. **518**(19): p. 5421-5425.
33. Irimia-Vladu, M. and J.W. Fergus, *Suitability of emeraldine base polyaniline-PVA composite film for carbon dioxide sensing*. Synthetic metals, 2006. **156**(21-24): p. 1401-1407.

34. Mathew, R., B.R. Mattes, and M.P. Espe, *A solid state NMR characterization of cross-linked polyaniline powder*. Synthetic Metals, 2002. **131**(1-3): p. 141-147.
35. Mu, S. and J. Kan, *Energy density and IR spectra of polyaniline synthesized electrochemically in the solutions of strong acids*. Synthetic metals, 1998. **98**(1): p. 51-55.
36. Matharu, Z., et al., *Polyaniline Langmuir– Blodgett film based cholesterol biosensor*. Langmuir, 2007. **23**(26): p. 13188-13192.
37. Huo, L., et al., *Preparation and characterization of doped polyaniline films*. Thin Solid Films, 1999. **350**(1-2): p. 5-9.
38. Li, A.Y., *Chemical origin of blue-and redshifted hydrogen bonds: Intramolecular hyperconjugation and its coupling with intermolecular hyperconjugation*. The Journal of chemical physics, 2007. **126**(15): p. 154102.
39. Wang, R.-X., L.-F. Huang, and X.-Y. Tian, *Understanding the protonation of polyaniline and polyaniline–graphene interaction*. The Journal of Physical Chemistry C, 2012. **116**(24): p. 13120-13126.
40. MacDiarmid, A.G. and A.J. Epstein, *Secondary doping in polyaniline*. Synthetic Metals, 1995. **69**(1-3): p. 85-92.
41. Manigandan, S., et al., *Formation of nanorods and nanoparticles of polyaniline using Langmuir Blodgett technique: Performance study for ammonia sensor*. Sensors and Actuators B: Chemical, 2008. **133**(1): p. 187-194.
42. *Veeco Dimension Icon with ScanAsyst Instrument Manual 004-1023-000*, V.I. Inc., Editor. 2010.

43. Clark Jr, L.C. and C. Lyons, *Electrode systems for continuous monitoring in cardiovascular surgery*. Annals of the New York Academy of sciences, 1962. **102**(1): p. 29-45.
44. Prince, S., *Characterization of electrodeposited polyaniline biosensor platform for Escherichia coli O157: H7 detection*. 2015.
45. Shrestha, R., D. Yang, and E. Irene, *Ellipsometry study of poly (o-methoxyaniline) thin films*. Thin Solid Films, 2006. **500**(1-2): p. 252-258.
46. Hale, J. and B. Johs, *CompleteEASE™ Data Analysis Manual*. 2011, Lincoln, Nebraska: JA Woollam Co., Inc.
47. Matharu, Z., et al., *Fundamentals and application of ordered molecular assemblies to affinity biosensing*. Chemical Society Reviews, 2012. **41**(3): p. 1363-1402.
48. Krukiewicz, K. and A. Katunin, *The effect of reaction medium on the conductivity and morphology of polyaniline doped with camphorsulfonic acid*. Synthetic Metals, 2016. **214**: p. 45-49.

### **3. Electrical Characteristics and Reversible Aging Effects in Polyaniline Thin Films Deposited by Langmuir-Blodgett Trough**

#### **3.1 Introduction**

Among the class of conductive polymers, polyaniline (PANi) is the most studied because of its many appealing characteristics, including its diverse oxidation states, tunable electrical conductivity, chemical and environmental stability, low-cost monomer source material, and its fully redox reversibility [1]. All of these novel properties of PANi result in many potential applications in biosensors [2], flexible (organic) solar cells [3], batteries [4], gas sensors [5], and super capacitors [6]. There are three known oxidation states for PANi: leucoemeraldine base (fully reduced), emeraldine base (half-oxidized), and pernigraniline base (fully oxidized). The emeraldine base is the most stable form of PANi and of great interest to the semiconductor industry as a conductive polymer because of its wide range of conductivity from insulator to fully conductive upon doping (protonation) [1].

In conductive polymers, it has been well established that structural disorder in the material reduces the efficient charge carrier transport and hence reduces the resulting device efficiency [7]. To address this problem, one strategy has been to align the polymer chains into a well-ordered quasi-two-dimensional (q2D) structure [7]. The Langmuir-Blodgett Trough (LB-Trough) method is a deposition technique which allows full control of molecular orientation and packing density in a q2D structure [8]. This technique allows a

self-assembly ordering of the PANi chains (molecules) in a monolayer at the air/water interface, which is transferable onto a substrate in a controlled condition [9].

Process optimization and electrical properties of LB-Trough deposited PANi film has been of interest to scientists for the last two decades. The conductivity of PANi depends on the oxidation state of the polymer and the degree of nitrogen atom protonation in the backbone chain [9]. Agbor compared the chemical structure and electrical properties of PANi among three deposition techniques for a gas (NH<sub>3</sub>) sensor application: spinning, evaporation, and LB-Trough. He showed LB-Trough deposited PANi film has the highest sensitivity among the tested techniques [10]. Cheung showed that molecular structure of LB PANi film is strongly influenced by the process aids used in mixture preparation. He reported a high level of conductivity at 50 – 100 S.m<sup>-1</sup> and showed that multilayer LB-PANi film using stearic acid (StA) as a process aid will result in homogeneous and phase-separated film, while a novel polyion (PI) complex of sulfonated polyaniline (SPAN) and stearylamine (StNH<sub>2</sub>) used as the processing aid will result in a high quality film [11]. Granholm et al. showed that the doping (protonation) level of LB-Trough PANi film can be controlled by adding protonic acids such as HCl or camphorsulfonic to the subphase. They demonstrated that adding neutral KCl salt to the subphase enhances the doping level up to 20 S.m<sup>-1</sup> when using HCl as protonic acid at room temperature [12]. Despite all the research that has been conducted on LB-Trough PANi film, little attention has been paid to the aging trend of this q2D structure conductive polymer film. Prokes et al. compared the aging effect of in-situ polymerized polyaniline film (a few μm thick) to that of polyaniline pellets (1 mm thick) and showed that PANi films lose their conductivity faster compared with bulk samples

[13]. Mostaani and coworkers studied the composite aging effect in bulk structure (1 mm thick) in polyaniline and polyaniline/multiwalled carbon nanotubes (PANi/MWCNTs) using a kinetic model and concluded that environmental air and moisture reacted with the polymer backbone [14].

We demonstrated earlier that commercially available lower molecular weights and shorter polymer chains of PANi source materials will produce the most successfully transferred uniform and homogeneous LB-Trough films compared to heavier and longer ones. In this study, an oxidative polymerization technique is used by maintaining the reaction temperature at 5 °C using ice bath to achieve the same molecular weight range based on data reported elsewhere [15]. Interdigitated electrodes (IDEs) at multiple electrode spacings are designed and fabricated on oxide-passivated silicon substrates for lateral DC conductivity measurements. Two doping methods, using an acidic (HCl) subphase during deposition and using an acidic redox dipping bath post deposition with a deionized water subphase as function of the hydrochloric acid molarity and time, are tested and the results are compared. The aging effect on the electrical conductivity is analyzed during a period of 30 days from deposition between the samples for both doping methods. The redox cycle and reversibility behavior of the film is also investigated.

## 3.2 Experimental

**Materials:** Aniline (C<sub>6</sub>H<sub>5</sub>NH<sub>2</sub>) ACS reagent ≥99.5%, chloroform (CHCl<sub>3</sub>) anhydrous ≥99%, containing 0.5 – 1.0% ethanol as a stabilizer, 1-Methyl-2-pyrrolidinone (C<sub>5</sub>H<sub>9</sub>NO) anhydrous 99.5%, known as NMP, and acetic acid (C<sub>2</sub>H<sub>4</sub>O<sub>2</sub>) reagent plus ≥99%, were

purchased from Sigma Aldrich and used as received. Ammonium Persulfate (APS)  $(\text{NH}_4)_2\text{S}_2\text{O}_8$  ACS reagent  $\geq 98\%$ , Hydrochloric acid (HCl) A144C-212 certified ACS plus 36.5 to 38%, and Whatman filter papers grade 4 with pore size 20 – 25  $\mu\text{m}$  were purchased from Fisher Scientific.

### **3.2.1 Polyaniline oxidative polymerization**

There are several studies presented in the literature focusing on the oxidative polymerization process of aniline in an acidic environment and its contributing parameters [16-18]. Mattoso and coworkers showed that the synthesis temperature has a direct impact on the molecular weight range of PANi. They demonstrated that maintaining the temperature between 3 and 5  $^{\circ}\text{C}$  will result in PANi with MWs averaging 20000  $\text{g}\cdot\text{mol}^{-1}$ , while lowering the temperature to  $-40^{\circ}\text{C}$  results in polymer molecular weights that can be as high as 417000  $\text{g}\cdot\text{mol}^{-1}$  [15]. Our past work that shows that lower PANi MWs are the most promising for uniform LB-Trough deposited thin films. Here, the synthesis media temperature was stabilized between 0 and 5  $^{\circ}\text{C}$  using an ice bath to achieve the lower molecular weights. As the first step of oxidative polymerization synthesis, 5 ml aniline was added to 75 ml of 1M HCl and stirred for 30 min to reach a transparent and homogenous solution. For the oxidizer, 2.875 g of Ammonium Persulfate (APS) was added to 50 ml of 1M HCl and cooled to a target 0  $^{\circ}\text{C}$ . Then, the APS mixture was added to the aniline mixture dropwise while stirring and maintaining the polymerization temperature below 5 $^{\circ}\text{C}$  using an ice bath. This step requires at least two hours to complete. Next, the mixture was filtered and the precipitate washed with 1 M HCl. The outcome is an emeraldine salt PANi cake. At this point, 500 ml 0.1M ammonium hydroxide was added, stirring for 48 h as a deprotonation step (emeraldine base). For the last step, the mixture was filtered and

rinsed with deionized water (18 M $\Omega$ cm) and dried under vacuum for 24 h at room temperature [15].

### **3.2.2 PANi LB trough deposition**

First, a mixture of 1:10 by weight of acetic acid : PANi was prepared. Then, 0.1 mg of the mixture was dissolved into 10 ml of NMP : Chloroform in a 5:1 volume ratio and sonicated for 90 minutes. Next, grade 4 Whatman filter papers were used to eliminate undissolved PANi particles. A 400  $\mu$ L of the solution was distributed uniformly over a LB-Trough (KSV-2000) at the air/water interface using micro-pipetting. A surface pressure against area per molecular unit isotherm graph was recorded using a platinum Wilhelmy plate. The surface pressure for film transfer was maintained at 30 mN/m. The barrier compression and deposition arm lifting speeds were maintained at 5 mm/min and 2 mm/min, respectively. A 1 min oxygen plasma cleaning and 3:1 H<sub>2</sub>SO<sub>4</sub>:H<sub>2</sub>O<sub>2</sub> piranha cleaning was applied on interdigitated electrodes and un-patterned (bare) oxidized silicon substrates respectively to produce consistent hydrophilic properties to the receiving surface prior deposition.

### **3.2.3 Doping**

Hydrochloric acid in different molarities was used for the doping (protonation) process of PANi by two methods. First, as a conventional method in LB-Trough deposition, an acidic subphase with desired molarity was used in the trough. Second, PANi films were deposited using a neutral deionized water subphase (pH=7) and the sample was dipped into an acidic bath of controlled molarity after deposition. The latter method is a suitable solution for substrates that might be damaged or otherwise impacted by an acidic subphase. Additionally, this post deposition process significantly reduces the volume of the chemical

usage depending on sample size. Various molarities and dipping times were tested by this method. Each sample was dried by 30 s of dry nitrogen flow prior to electrical measurement.

### **3.2.4 Electrical conductivity study**

Interdigitated Electrodes (IDEs) were fabricated in the Michigan Technological University Microfabrication Facilities (MFF) on 100 mm diameter single-side polished <100> *p*-type silicon substrates with 8 – 12  $\Omega$ /cm electrical resistivity (WRS materials). A 160±5 nm silicon dioxide layer was thermally grown at 1100 °C using a Mellen Clamshell furnace under dry environmental conditions and 3 SLM O<sub>2</sub> flow for two hours as an electrical insulation layer. A subtractive (etching) process was used for the IDEs patterning, which produces more uniform electrode patterns and dimensional profiles compared to a lift-off technique, considering the long (3.5 mm) and thin (20  $\mu$ m) IDEs fingers (Figure 3. 1).

First, the silicon wafer was cleaned in a “piranha” solution (3:1, H<sub>2</sub>SO<sub>4</sub>: H<sub>2</sub>O<sub>2</sub>) for 20 minutes. Next, a Cr/Au stack, with thickness of 5 nm/30 nm respectively, was deposited using an *e*-beam evaporation system (Denton DV-502A). The thin layer of chromium was deposited as a common adhesion layer between the gold and silicon dioxide films [19]. Next, a positive photoresist (Shipley S1813) was spun at 4000 rpm for 40 s resulting in a 1.3  $\mu$ m uniform photoresist film layer followed by soft bake at 115 °C for 60 s to drive of any remaining solvents from the film. A 125 mm bright field photolithographic mask (designed in KLayout V 0.25.9) was used to transfer the designed pattern from the mask to the substrate. The photoresist (with a exposure dose of 170 mJ/cm<sup>2</sup>) was aligned and

exposed for 24.9 s using the EVG-620 mask aligner instrument using a 365 nm UV source at an average lamp intensity of  $6.82 \text{ W/cm}^2$ . Then, the photoresist was developed for 40 s using MF-319 developer followed by gold etchant TFA (etch rate  $28 \text{ \AA/s}$ ) and CR-7 chromium etchant (etch rate  $24 \text{ \AA/s}$ ). For the last step, the photoresist was removed using acetone, isopropanol alcohol, followed by a deionized water rinse prior to dicing the wafer to the test die dimensions  $5 \text{ mm} \times 20 \text{ mm}$  (Figure 3. 1) using a Microautomation MA 1000 dicing saw. For all electrical measurements, a Keithley 4200A-SCS semiconductor characterization system and a Micromanipulator probe station with shielded micromanipulators has been utilized.

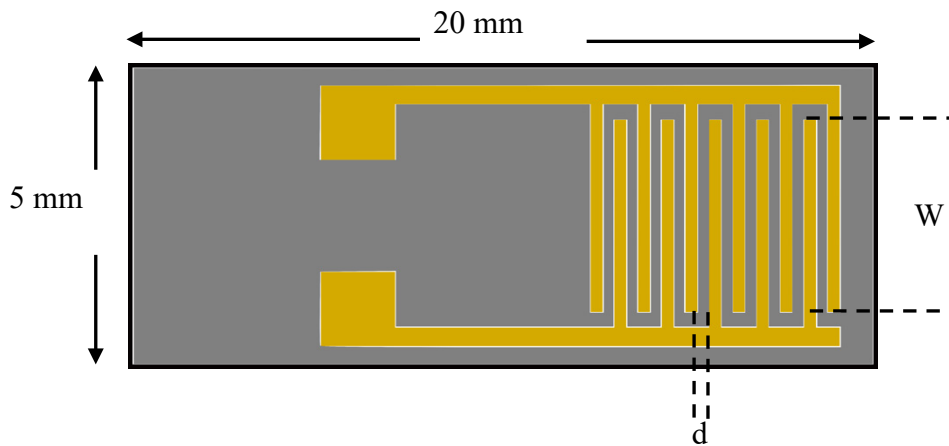


Figure 3. 1 Sketch of an interdigitated electrode array used in this study. Electrodes were fabricated in Cr/Au, 5nm/30nm thickness respectively on a 160 nm thermally grown oxide layer on silicon substrate:  $d$  = spacing between fingers and  $w$  = fingers overlay length

### 3.2.5 SEM images

For the physical surface morphology, a Hitachi S-4700 field-emission scanning electron microscope (FE-SEM) was used. A 2 nm carbon coating was applied using a high vacuum evaporation system for each sample prior to the SEM imaging.

## 3.3 Results and Discussion

The electrical conductivity,  $\sigma$ , of LB-Trough deposited PANi film was measured as a function of hydrochloric acid molarity for both doping methods investigated in this study. Films deposited with an acidic subphase and those deposited using a neutral subphase and protonated using a post-deposition acidic dip exposure. The current-voltage characteristics of the films were measured using interdigitated electrodes (IDEs), and all data were collected in the linear ohmic resistance region. The conductivity was calculated based on the IDEs geometrics and dimensions, PANi film thickness, and the applied voltage:

$$\sigma = \frac{I \cdot d}{w \cdot t \cdot V}$$

where  $I$  is the measured current,  $d$  is the electrodes spacing,  $w$  is the electrode fingers overlay length (3.2 mm),  $t$  is the PANi film thickness, and  $V$  is the applied voltage (Figure 3. 1) [20]. To investigate the linearity and the ohmic contact, interdigitated electrodes with different spacings (20, 50, and 100  $\mu\text{m}$ ) and different PANi film thicknesses were tested. For the film thickness measurement, atomic force microscopy (Bruker Dimension ICON AFM) was used for step analysis and confirmed using ellipsometry (J.A. Woollam V-VASE) over the wavelength range of 300 – 1500 nm at three different incident angles of

65°, 70°, and 75° using a Cauchy fitting model. The data showed that the LB-Trough PANi film deposition produced approximately 2 nm per layer on average, which is in agreement with previous studies [7, 10].

Figure 3. 2 shows the change in conductivity against the subphase HCl molarity (neutral, 0.1, 0.5, 1, 1.5, 2, and 2.5 M HCl). A logarithmic scale is used for the y-axis because of significant changes in conductivity due to the protonation process. For the undoped PANi, the conductivity was found to be  $5.2 \times 10^{-6}$  S/m which is slightly higher than previously reported values for undoped emeraldine base PANi films at  $10^{-7}$  S/m [21]. This small conductivity increase for undoped LB-Trough-deposited PANi film has been attributed to low-level doping by acetic acid in the mixture preparation in past studies [10]. By increasing the subphase acidity (HCl), the conductivity increased more than six orders of magnitude and peaked at 4.56 S/m for the 1.5 M HCl subphase. Interestingly, increasing the subphase molarity beyond 1.5 M, had an inverse impact on the conductivity. The conductivity reduced to  $1.3 \times 10^{-3}$  S/m for 2.5 M HCl. This is a known electrical behavior for polyaniline and previously reported in the literature [22]. Unlike other conductive polymers, whose conductivity increases and reaches a saturation level through a higher doping concentration, PANi first reaches high conductivity at the intermediate oxidation state and then reduces back to a nonconductive state at higher doping levels [22]. In fact, PANi is not conductive for low doping levels; it transitions to a conducting polymer at intermediate doping concentrations and returns to a nonconductive state at high doping concentrations [22].

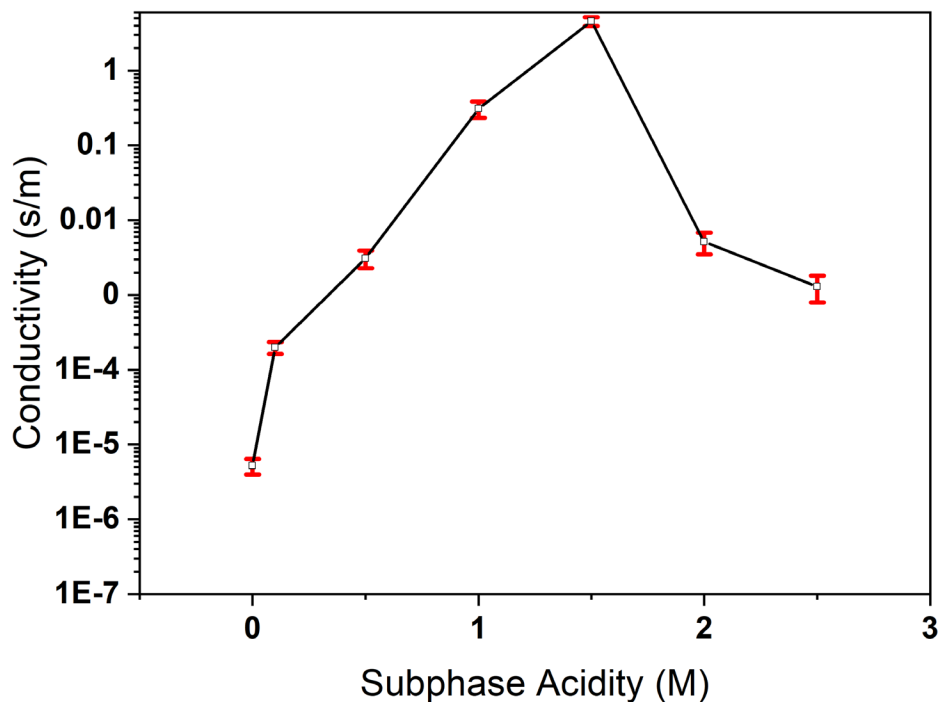


Figure 3. 2 Semi-log plot of the electrical conductivity versus hydrochloric molarity (neutral, 0.1, 0.5, 1, 1.5, 2, 2.5 M HCl) as a subphase of LB-Trough deposited PANi film on interdigitated electrodes (IDEs)

The changes in conductivity as a function of the time and protonic acid (HCl) molarity for LB-Trough deposited PANi films using neutral deionized water (18 MΩcm) as the deposition subphase and employing a post-deposition doping treatment by dipping the specimen in hydrochloric acid bath are shown in Figure 3. 3a. The graph indicates that conductivity increased with the acid molarity and reached to its highest value at 41 S/m for 1.5 HCl and decreased, again, when stronger acid baths were applied. A similar trend was seen using the acidic subphase deposition method (Figure 3. 2). Data indicate that the conductivity increased exponentially during the first 10 minutes and then reached its saturated level. Figure 3. 3b shows the current-voltage data of a 45 layer LB-Trough-

deposited PANi film on an interdigitated electrode with 100  $\mu\text{m}$  spacing between the electrodes as a function of the dipping time in an acidic bath (1.5 M HCl). The data linearity confirms the ohmic contact between the PANi film and the electrodes. Each interdigitated electrode sample was tested for electrical characteristics prior to deposition to avoid any potential short circuit contact between the electrodes as a result of defects introduced in the lithography or etch steps.

Comparing the two doping methods under study here shows that one order of magnitude higher conductivity was achieved using a dipping bath method compared to an acidic subphase deposition technique for the same doping concentration (1.5 M HCl), 4.56 S/m vs 41 S/m, respectively (Figures 3. 2 & 3a). To have a better understanding of the nanostructure of the LB-Trough-deposited PANi films and a comparison between the two doping methods tested here, scanning electron microscopy (SEM) has been used.

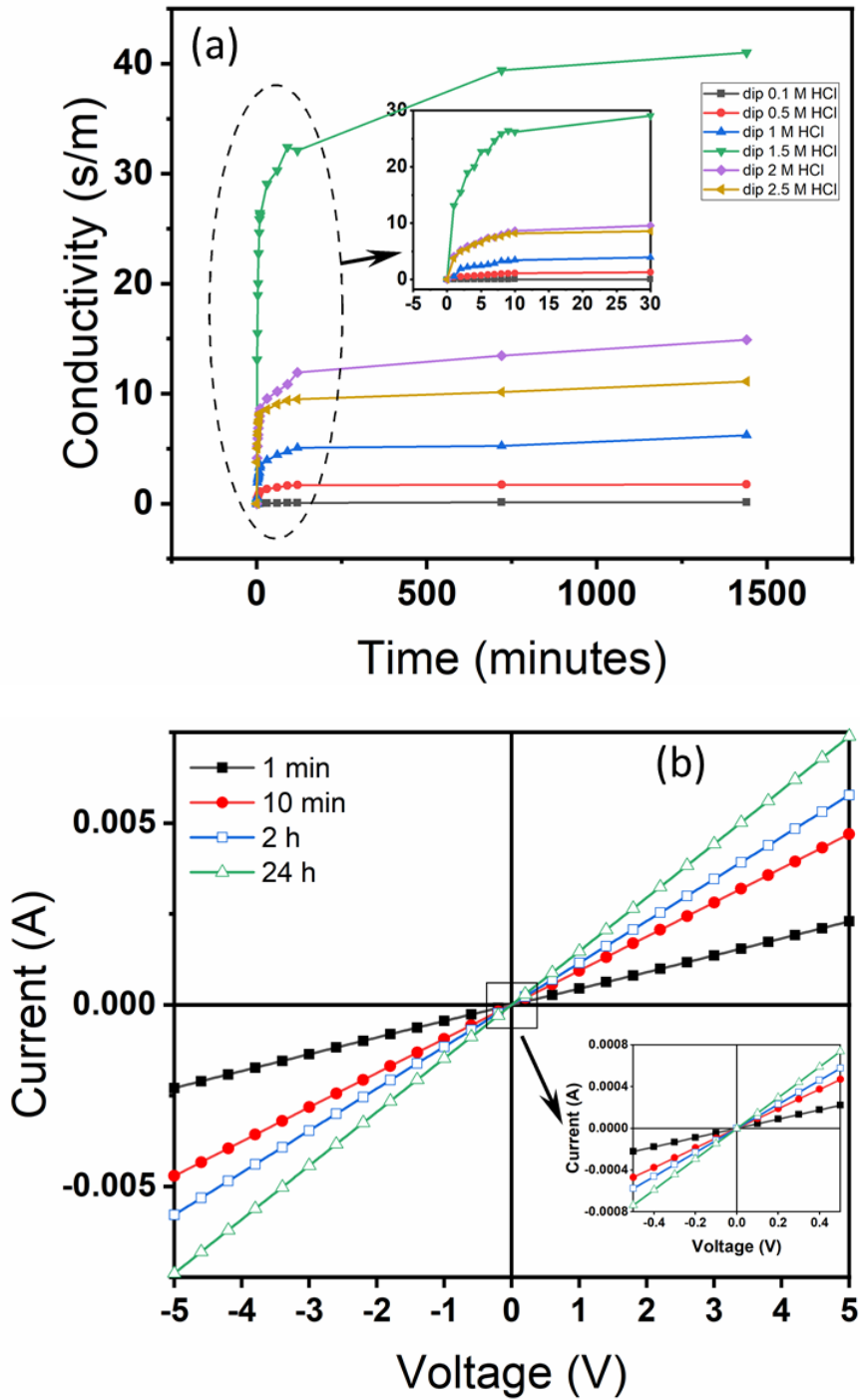


Figure 3. 3 The room-temperature electrical properties of 45 layers LB-Trough-deposited PANi film on interdigitated gold electrodes on a silicon substrate post-deposition doping process by dipping in acidic bath (HCl), (a) Conductivity variation as function of hydrochloric acid molarity and time, (b) current vs. voltage characteristics as function of dipping time: 1 min, 10 min, 2 h and 24 h.

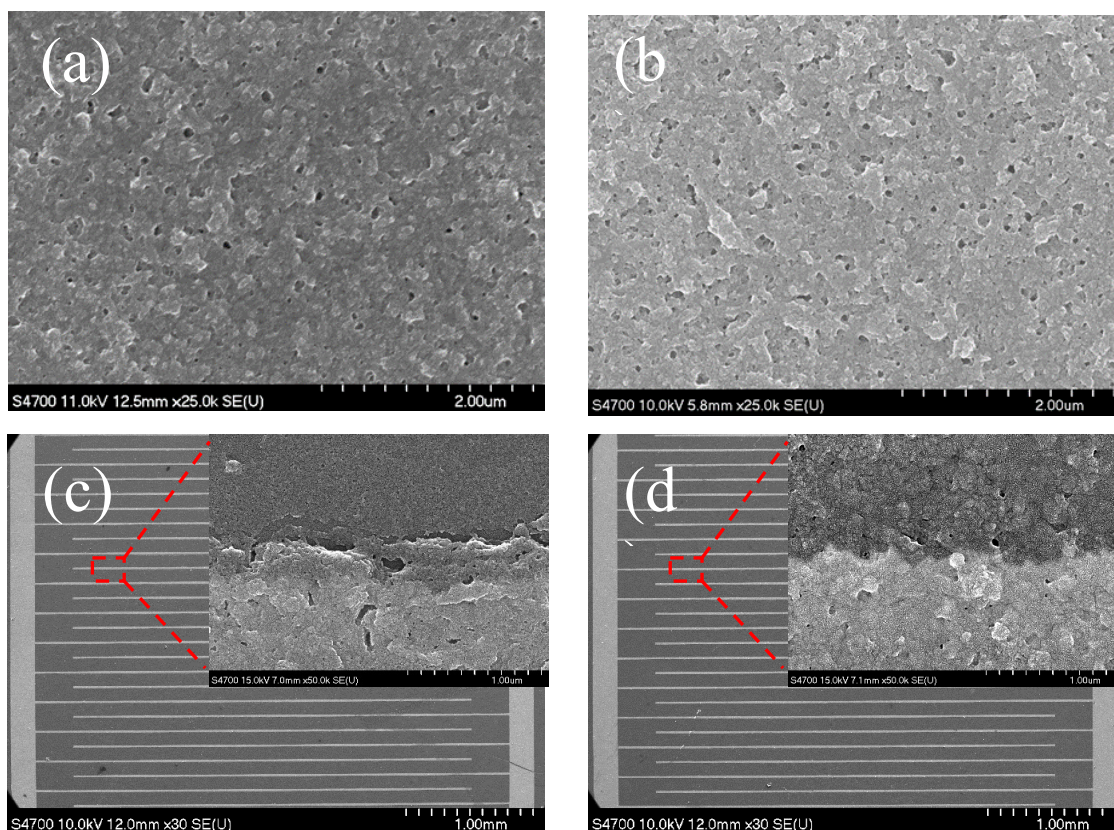


Figure 3. 4 SEM images of 45 layers LB-Trough-deposited PANi films on (a)(b) silicon substrates with 160 nm oxide layer, (c)(d) interdigitated electrodes (30-nm Au on 5-nm Cr) fabricated on a (100) Si substrate covered by 160 nm thermal oxide. Each electrode finger is 20- $\mu$ m wide and the gaps between the electrodes are 100- $\mu$ m. (a) undoped PANi film using neutral deionized water subphase (b)(c) doped PANi film using acidic subphase, 1.5 M HCl (d) doped PANi film using deionized water neutral subphase and acidic bath, 1.5 M HCl for 24 h. The inset images show PANi film at the border of electrode.

The morphology of doped and undoped LB-Trough-deposited PANi film on bare silicon substrates and interdigitated electrodes are shown in Figure 3. 4. The SEM images of silicon substrates indicated that both undoped and doped PANi films using deionized water and 1.5 M HCl subphases, respectively, have the same uniform porous nanostructure and network (Figure 3. 4a and 4b). Conversely, there are some non-homogenous or discontinuity issues for PANi film deposited on IDEs at the electrode edge using an acidic

subphase (Figure 3. 4c). This can be attributed to the wettability surface property variation of gold electrode versus silicon dioxide in acidic media (hydrochloric acid in this case). It is known that the hydrophilic properties of a substrate surface are a key factor in LB-Trough PANi film deposition [10, 20]. From our prior experience, silicon dioxide should have lost its hydrophilic properties in acidic media after a few layers of deposition, but the gold electrode preserves its hydrophilic behavior. A further detailed surface analysis is required in future work to confirm this hypothesis. The PANi film discontinuity on interdigitated electrodes could be a significant contribution to the lower conductivity in samples that use an acidic subphase in LB-Trough deposition compared to those that use a neutral subphase and acid bath dip method post-deposition.

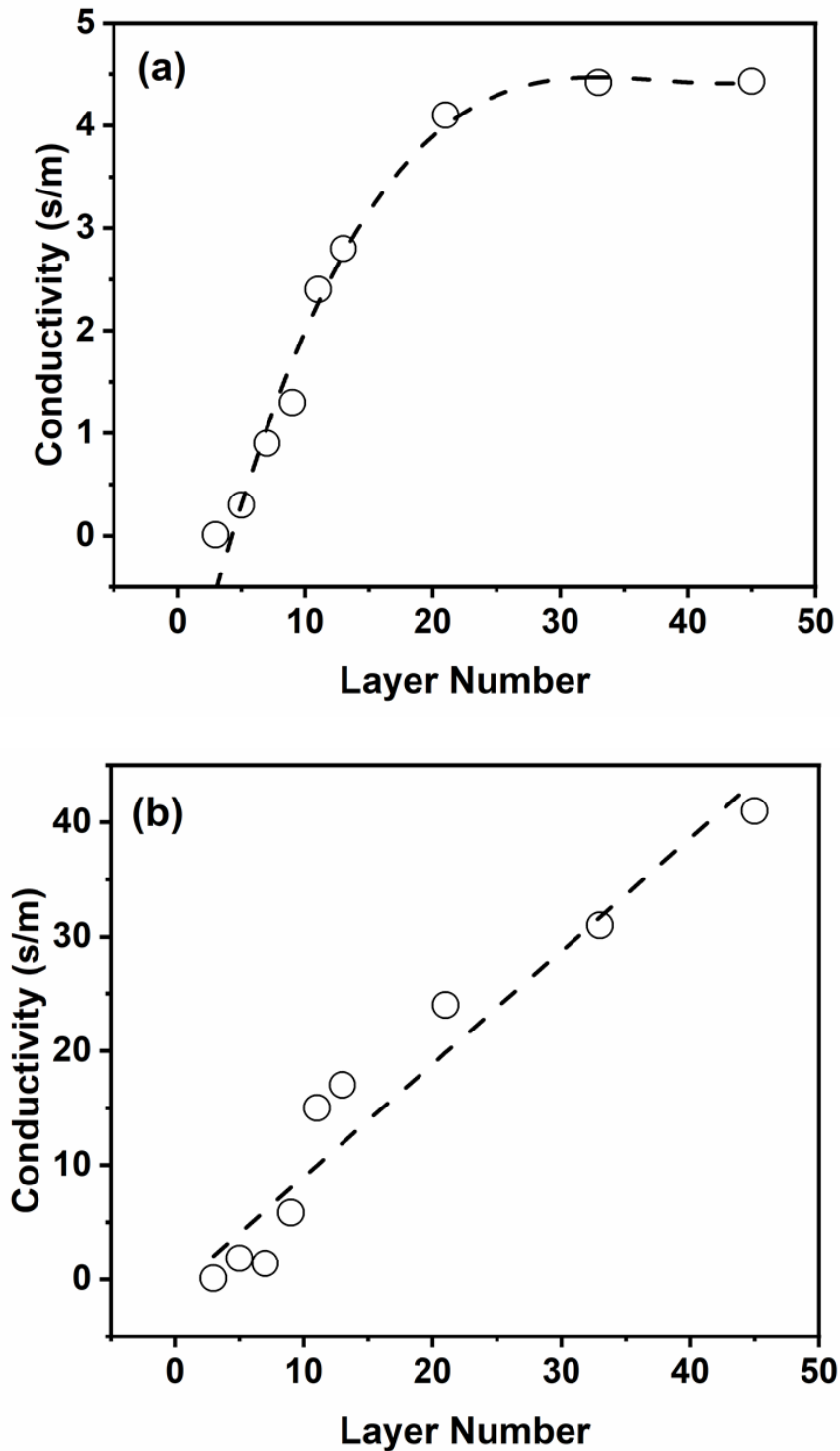


Figure 3. 5 In-plane electrical conductivity versus the number of single layer LB-Trough transferred PANi film: (a) employing 1.5 M HCl subphase, (b) using neutral subphase for deposition and using 1.5 M HCl dipping bath for 24 h post deposition. The slopes on the graphs are 0.25 and 1 for the linear portion of the (a) and (b) graphs respectively.

The impact of the PANi film thickness on its conductivity was also studied. Figure 3. 5 shows the change in conductivity with number of layers (3 to 45 layers) when using 1.5 M HCl acidic subphase (Figure 3. 5a), and the post-LB-Trough deposition doping treatment with an acidic bath (Figure 3. 5b). For the acidic subphase, the conductivity increased linearly up to 21 layers and saturated around 4.5 s/m. However, the conductivity increased linearly for up to 45 layers tested here when using the neutral subphase for deposition and then dipping in acidic bath (1.5 M HCl) post deposition for 24 h. This data confirms the direct impact of the film thickness on the lateral conductivity. Combining the discoveries from the SEM images (Figure 3. 4) with the conductivity results based on the layer numbers (Figure 3. 5), it can be realized that the main reason for lower conductivity for the acidic subphase doping method must be because of the PANi film discontinuity after a certain number of deposited monolayers. The conductivity slope for graphs in the linear regions of Figure 3. 5a and 5b are 0.25 and 1, respectively. This information indicates that using an acidic subphase as the doping method will result in a lower protonation in general, compared to other methods tested here, apart from the PANi film discontinuity issue on the thicker films. This can be because of an aging effect on electrical conductivity. Each single layer deposited in this method air dried for 30 minutes before next layer deposition.

To obtain charge carrier information, which is critical for application of the film in devices, and in order to validate the conductivity data obtained by the IDEs, a Hall effect measurement (Ecopia HMS-3000) was used for the PANi films the neutral subphase deposition plus post-deposition doping method at three different HCl concentrations. The

results of this study are shown in Table 1. The dimensions of the specimens were 0.5 cm × 0.5 cm with an excitation current of 1 μA and constant magnetic field of 0.55T. It was found that the conductivity measured by IDEs was very close to those measured by the Hall effect, with slightly lower values, which could be due to contact resistance on the IDEs. The carrier density and mobility data reported here are slightly higher than values reported by Sengupta [23], where the deposition method involved casting the mixture on a glass substrate. This improvement could be due to having a quasi-two-dimensional and more ordered structure for the LB-Trough PANi films used in this study.

Table 3. 1 Conductivity, carrier density, and mobility of HCl doped LB-Trough PANi films

HCl molarity	Conductivity (s/m)		Carrier density (cm <sup>-3</sup> )	Carrier mobility (cm <sup>2</sup> V <sup>-1</sup> s <sup>-1</sup> )
	IDEs	Hall Effect		
0.5	1.75	1.96	3.41×10 <sup>17</sup>	39.19
1.5	41.01	43.57	1.08×10 <sup>18</sup>	57.08
2.5	11.17	12.08	8.83×10 <sup>17</sup>	41.97

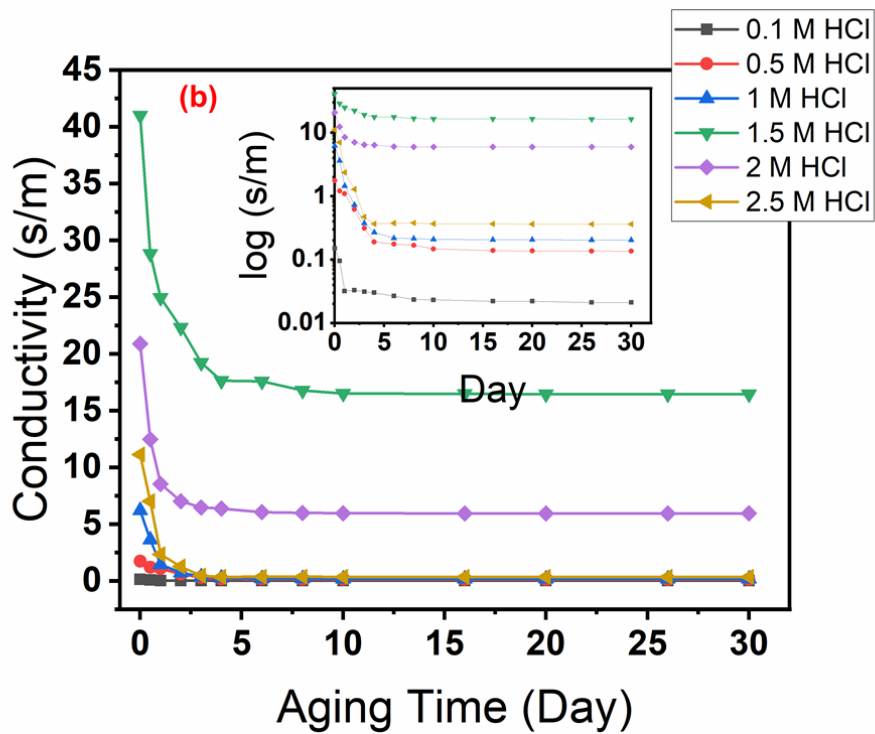
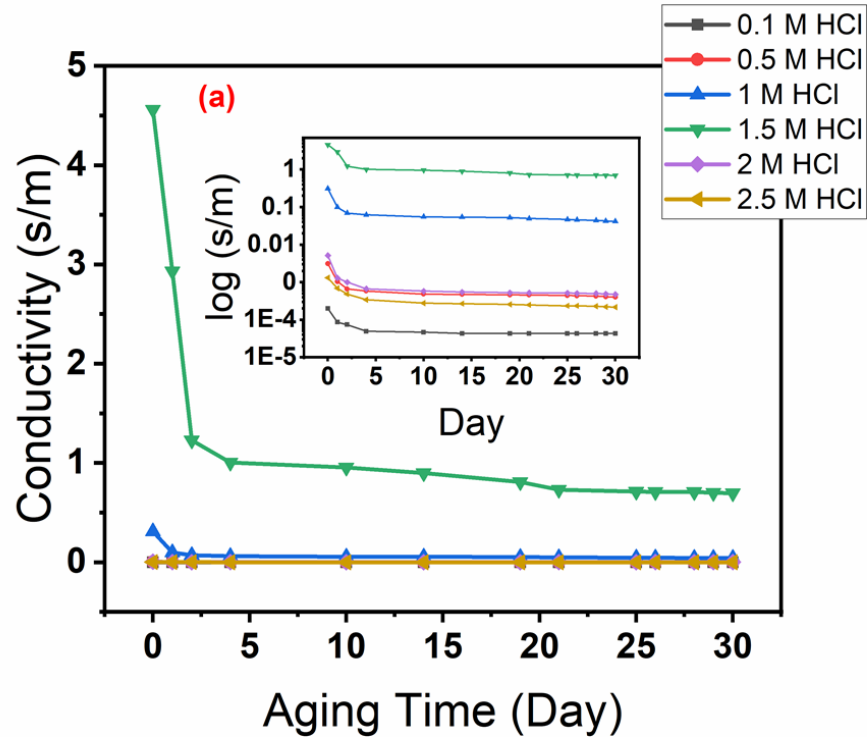


Figure 3. 6 Electrical conductivity of 45 layers LB-Trough-deposited PANi film versus aging time for (a) employing 1.5 M HCl subphase, (b) using neutral subphase for deposition and using 1.5 M HCl bath for doping.

Figure 3. 6 shows the conductivity changes during the storage time (aging) under laboratory conditions for both doping methods under study. Data shows a steep decline in conductivity during the first 2–4 days that stabilized after approximately 5 days for both doping methods. On average, the conductivity dropped only 2% during the next 25 days once it reached its steady state. Three factors are considered to be responsible for polyaniline conductivity decay over time. The first factor is the loss of absorbed moisture from processing [24]. This effect is likely to have a stronger impact at elevated temperatures ( $>100^{\circ}\text{C}$ ) but less so at room temperature. The second process is oxidative degradation, which is due to the oxygen and water vapor in the air reacting with the polyaniline chain backbone [25]. This is known to be a very slow process for polyaniline and is not reversible. The third is a gradual deprotonation in the interactions with the ambient environment, which is reversible. This aging mechanism, which behaves like a diffusion process, initiates from the conducting PANi surface and expands through the conductive ordered grains. Prokes et al. showed that the deprotonation process is faster for PANi films (a few micrometers thick) compared to the compressed pellets (a few millimeters thick) [13]. Here, the dominant aging process is attributed to gradual deprotonation due to the ultrathin nature of the LB-Trough deposited PANi film.

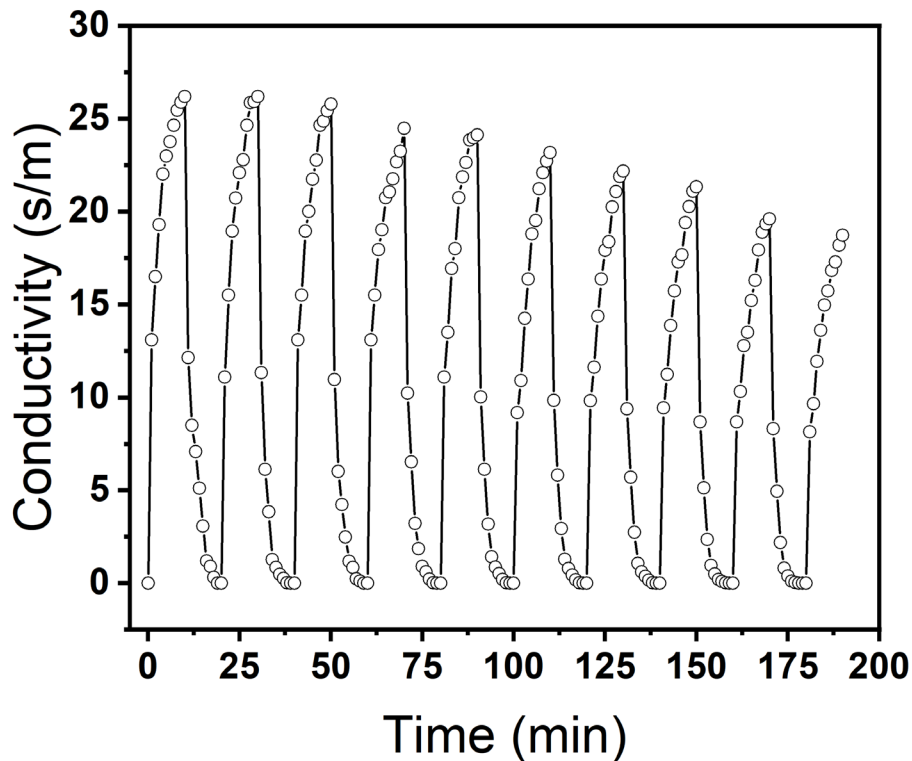


Figure 3. 7 Response and recovery time of 45 layers LB-Trough-deposited PANi film to 0.1 M  $\text{NH}_4\text{OH}$ . Sample was dipped in 1.5 M HCl for the recovery process.

To test this third aging mechanism, the LB-Trough-deposited PANi film with a neutral (deionized water) subphase was used to investigate the redox cycling behavior of the film, which also has wide applications in gas and pH sensors [26, 27] (Figure 3. 7). For this purpose, 45 layers of PANi film deposited on IDEs substrate was dipped in 1.5 M HCl for the doping (recovery) process and dipped in 0.1 M  $\text{NH}_4\text{OH}$  for the reduction (sensing) process for 10 minutes on each step. The decrease in conductivity through exposure to the ammonium hydroxide is due to a reduction of  $\text{H}^+$  holes from the nitrogen atoms in the PANi film structure. By repeating the redox cycle 10 times, the sample recovered 72% of

its original conductivity. The loss of original conductivity in the redox cycling process is attributed to the changes that oxidation and reduction process will make to the PANi backbone chain [28]. The recovery is due to protonating the polymer by exposure to HCl. The average response time for the protonation and reduction process to reach 90% of saturated values was 5 and 4.5 minutes respectively.

### **3.4 Conclusions**

In this study, we have synthesized polyaniline in emeraldine base form using oxidative polymerization. We designed, fabricated, and utilized interdigitated electrodes on an oxide passivated silicon substrate for DC electrical characterization of the films. The LB-Trough layer-by-layer deposition technique has been used to deposit ultrathin q2D PANi films on a silicon substrate with two subphase conditions. Two doping methods were investigated: acidic (HCl) subphase and an acidic dip post-deposition process as a function of acid molarity and time. The highest conductivity ( $41 \text{ S.m}^{-1}$ ) was achieved using the acidic (1.5 M HCl) dip method for 24 hours. Scanning electron microscopy (SEM) was used to study the impact of the process conditions on the morphology and nanostructure of the films. The SEM images showed uniform porous nano-structured PANi films on unpatterned oxide passivated silicon substrates and also indicated that there are PANi film inhomogeneity issues at the IDEs electrode edge for samples using an acidic subphase, eventually reducing the effective PANi film thickness for charge transport at that boundary. The electrical conductivity aging data exhibited a steep drop in conductivity for the first 5 days before reaching its steady state. The minimum conductivity loss was 50% during the first 5 days, however it showed itself to be stable after that (less than 2% drop in conductivity over next 25 days). The reversibility (redox cycle) test revealed that LB-Trough PANi film recovered

72% of its initial conductivity after 10 cycles, indicating long term changes to the PANi backbone chain when undergoing these extreme cycles.

The presented study is a part of ongoing research for biosensor applications. The electrical characteristics of LB-Trough PANi films presented here will impact the device design analysis in applications where the PANi film serves as part of an active sensing layer of the device. Future studies remain for polyaniline ultrathin film behavior for interaction with other films and packaging materials.

### **3.5 Acknowledgements**

This work was supported by funding from Michigan Technological University, through the College of Engineering and the Department of Electrical and Computer Engineering. The authors gratefully acknowledge support from the Microfabrication Facility and the Applied Chemical and Morphological Analysis Laboratory at Michigan Technological University for the processing and characterization capabilities utilized in this study.

### 3.6 References

1. Bhadra, S., et al., *Progress in preparation, processing and applications of polyaniline*. Progress in polymer science, 2009. **34**(8): p. 783-810.
2. Dhand, C., et al., *Recent advances in polyaniline based biosensors*. Biosensors and Bioelectronics, 2011. **26**(6): p. 2811-2821.
3. Salvatierra, R.V., et al., *ITO-free and flexible organic photovoltaic device based on high transparent and conductive polyaniline/carbon nanotube thin films*. Advanced Functional Materials, 2013. **23**(12): p. 1490-1499.
4. Luo, Y., et al., *Application of polyaniline for Li-ion batteries, lithium-sulfur batteries, and supercapacitors*. ChemSusChem, 2019. **12**(8): p. 1591-1611.
5. Fratoddi, I., et al., *Chemiresistive polyaniline-based gas sensors: A mini review*. Sensors and Actuators B: Chemical, 2015. **220**: p. 534-548.
6. Eftekhari, A., L. Li, and Y. Yang, *Polyaniline supercapacitors*. Journal of Power Sources, 2017. **347**: p. 86-107.
7. Zhang, T., et al., *Engineering crystalline quasi-two-dimensional polyaniline thin film with enhanced electrical and chemiresistive sensing performances*. Nature communications, 2019. **10**(1): p. 1-9.
8. Hupfer, M.L., et al., *Supramolecular Reorientation During Deposition Onto Metal Surfaces of Quasi-Two-Dimensional Langmuir Monolayers Composed of Bifunctional Amphiphilic, Twisted Perylenes*. Langmuir, 2021. **37**(37): p. 11018-11026.

9. Paddeu, S., M.K. Ram, and C. Nicolini, *Investigation of ultrathin films of processable poly (o-anisidine) conducting polymer obtained by the Langmuir–Blodgett technique*. The Journal of Physical Chemistry B, 1997. **101**(24): p. 4759-4766.
10. Agbor, N., M. Petty, and A. Monkman, *Polyaniline thin films for gas sensing*. Sensors and Actuators B: Chemical, 1995. **28**(3): p. 173-179.
11. Cheung, J. and M. Rubner, *Fabrication of electrically conductive Langmuir–Blodgett multilayer films of polyaniline*. Thin Solid Films, 1994. **244**(1-2): p. 990-994.
12. Granholm, P., J. Paloheimo, and H. Stubb, *Langmuir-Blodgett films of polyaniline: Fabrication and transport studies*. Physical Review B, 1997. **55**(20): p. 13658.
13. Prokeš, J., et al., *Conductivity of polyaniline films during temperature cycling*. Synthetic metals, 2001. **1**(119): p. 479-480.
14. Mostaani, F., M. Moghbeli, and H. Karimian, *Electrical conductivity, aging behavior, and electromagnetic interference (EMI) shielding properties of polyaniline/MWCNT nanocomposites*. Journal of Thermoplastic Composite Materials, 2018. **31**(10): p. 1393-1415.
15. Mattoso, L.H., A.G. MacDiarmid, and A.J. Epstein, *Controlled synthesis of high molecular weight polyaniline and poly (o-methoxyaniline)*. Synthetic Metals, 1994. **68**(1): p. 1-11.
16. MacDiarmid, A.G. and A.J. Epstein, *Secondary doping in polyaniline*. Synthetic Metals, 1995. **69**(1-3): p. 85-92.

17. Leclerc, M., J. Guay, and L.H. Dao, *Synthesis and characterization of poly (alkylanilines)*. *Macromolecules*, 1989. **22**(2): p. 649-653.
18. Butoi, B., et al., *Morphological and Structural Analysis of Polyaniline and Poly (O-anisidine) Layers Generated in a DC Glow Discharge Plasma by Using an Oblique Angle Electrode Deposition Configuration*. 2017. **9**(12): p. 732.
19. Sapsanis, C., et al., *Insights on capacitive interdigitated electrodes coated with MOF thin films: Humidity and VOCs sensing as a case study*. *Sensors*, 2015. **15**(8): p. 18153-18166.
20. Logsdon, P.B., J. Pfleger, and P.N. Prasad, *Conductive and optically non-linear polymeric Langmuir-Blodgett films of poly (3-dodecylthiophene)*. *Synthetic metals*, 1988. **26**(4): p. 369-381.
21. Yagudaeva, E., et al., *Tetramer of aniline as a structural analog of polyaniline— Promising material for biomedical application*. *Synthetic Metals*, 2021. **274**: p. 116712.
22. McManus, P.M., R.J. Cushman, and S.C. Yang, *Influence of oxidation and protonation on the electrical conductivity of polyaniline*. *Journal of Physical Chemistry*, 1987. **91**(3): p. 744-747.
23. Sengupta, P.P. and B. Adhikari, *Influence of polymerization condition on the electrical conductivity and gas sensing properties of polyaniline*. *Materials Science and Engineering: A*, 2007. **459**(1-2): p. 278-285.
24. Kukla, A., Y.M. Shirshov, and S. Piletsky, *Ammonia sensors based on sensitive polyaniline films*. *Sensors and Actuators B: Chemical*, 1996. **37**(3): p. 135-140.

25. Kim, S. and I.J. Chung, *Annealing effect on the electrochemical property of polyaniline complexed with various acids*. Synthetic metals, 1998. **97**(2): p. 127-133.
26. Sharma, A.L., K. Kumar, and A. Deep, *Nanostructured polyaniline films on silicon for sensitive sensing of ammonia*. Sensors and Actuators A: Physical, 2013. **198**: p. 107-112.
27. Matharu, Z., et al., *Fundamentals and application of ordered molecular assemblies to affinity biosensing*. Chemical Society Reviews, 2012. **41**(3): p. 1363-1402.
28. Wang, J., et al., *Electrochemically fabricated polyaniline nanoframework electrode junctions that function as resistive sensors*. Nano Letters, 2004. **4**(9): p. 1693-1697.

## 4. Conclusion and Future works

### 4.1 Conclusion

Three objectives were outlined for the research scope of this dissertation. The first goal was to optimize and develop a LB-Trough deposition process for a uniform and reproducible PANi film at the nanoscale. In this regard, three molecular weights of commercially available EB-PANi (5000, 50000, 100000 g.mol<sup>-1</sup>) were studied with two subphase conditions (deionized water, 2 M HCl acidic subphase) and under two commonly utilized mixture preparation recipes from the literature. The FTIR absorption spectra peaks assignment revealed PANi thin film formation and an expected blue shift of the PANi signature peaks between 1700 cm<sup>-1</sup> and 1100 cm<sup>-1</sup>, confirming film protonation for the 2 M HCl subphase condition. Spectroscopic ellipsometry and atomic force microscopy were used to determine and confirm the film thickness and surface roughness measurements for LB-Trough-based PANi. Demonstrated reproducibility of the mixture using NMP + Chloroform as solvents with a source PANi molecular weight of 5000 g.mol<sup>-1</sup> is presented as a promising thin film deposition condition in terms of film quality, excellent thickness control with 1.1 – 2.2 nm/layer depending on subphase conditions, while producing a uniform and homogenous film. Thin film surface roughness measurements revealed a smoother film by a factor of two for the undoped versus subphase-doped film deposition conditions. By monitoring the LB-trough thin film deposition transfer ratio and film thickness measurements using AFM and ellipsometry, the study confirmed Z-type deposition for the undoped (DIW subphase) and Y-type deposition for the doped (2M HCl subphase) LB-trough EB-PANi films.

The second goal was to study the electrical properties of LB-Trough deposited PANi film and investigate the film's aging behavior on electrical conductivity. Since the commercial 5000 g.mol<sup>-1</sup> EB-PANI exhibited very poor conductivity in DC electrical measurements, not as expected for emeraldine-base PANi films, an oxidative polymerization process was used to synthesize an EB-PANI source material following a well-characterized recipe under conditions that would produce a targeted 5000 g.mol<sup>-1</sup> molecular weight. Interdigitated electrodes (IDEs) were designed and fabricated for electrical conductivity measurements on an oxide-passivated silicon substrate. Two doping methods were investigated, an acidic (HCl) subphase and an acidic dip post-deposition process as a function of solution molarity and time. The highest conductivity (41 S.m<sup>-1</sup>) was achieved using the acidic (1.5 M HCl) dip doping method for 24 hours. Scanning electron microscopy (SEM) was used to confirm the morphology and nanostructure of the PANi film. SEM images showed uniform porous nanostructured PANi film on a bare silicon substrate and indicated PANi film inhomogeneity issues at the IDEs gold electrode edge for samples using the acidic subphase, resulting in lowering the effective PANi film thickness for the charge transport. The electrical conductivity aging data showed a steep drop in conductivity during the first 5 days before reaching its steady state. The minimum conductivity loss was 50% during the first 5 days; however, the conductivity stabilized after the initial loss, resulting in a change of less than a 2% drop in conductivity over the next 25 days.

The third goal was to demonstrate the LB-Trough deposited PANi film applications in electrochemical and biochemical sensing. In this regard, 45 layers LB-Trough deposited PANi film on interdigitated electrodes with a neutral subphase was used as a pH sensor by monitoring the film's redox cycling behavior. The doping and reducing process (redox

cycling) was repeated 10 times with 1.5 M HCl and 0.1 M NH<sub>4</sub>OH, respectively. Data showed 72% of the initial conductivity of LB-Trough deposited PANi film was recovered after 10 redox cycling. The average response time for the protonation and reduction process to reach its 90% of saturated values was 5 and 4.5 minutes, respectively. The loss of original conductivity in the redox cycling process is attributed to the oxidation and reduction process changes to the PANi backbone chain.

## **4.2 Future Work**

In the LB-Trough PANi deposition development project, collected data showed a Z-type deposition for a neutral subphase versus a Y-type deposition for an acidic subphase. A further study is required to more completely understand this mechanism, and to investigate if there is any similar behavior for any other LB-Trough deposited polymer films. In addition, because of the film orientation differences between Z-type (tail-to-head) and Y-type (tail-to-tail and head-to-head) Figure 1.4 , this can potentially impact the physical, electrical, and optical properties of the film, which require further investigations.

Between the two mixture preparation recipes tested in this work, NMP + Chloroform showed a successful LB-Trough deposition for more than 55 layers; however, using NMP only as the solvent could deposit a film up to 5 layers based on the LB-Trough transfer ratio data. From a LB-Trough deposition process development point of view, the impact of the NMP only as the solvent on the PANi chain structure needs additional work to be fully understood. Fourier transform infrared spectroscopy (FTIR), scanning electron microscopy (SEM), and transfer electron microscopy (TEM) are recommended as characterization

techniques to collect more bonding structure, surface morphology, and polymer orientation data, respectively.

The presented work is part of ongoing research for biosensor applications. Binding a biochemical antigen protein to the LB-PANi surface enables the film to serve as a sensor for nonreversible binding events between antigen and antibody molecules when and if the binding events inhibit the transfer of charge in the interdigitated electrode arrays. The electrical characteristics of LB-Trough PANi film presented here will enable device design evaluation by having the PANi film as an active conducting layer in the device. Future studies still need to be done in polyaniline ultrathin film behavior in interaction with other layers and packaging materials.

## **A Appendix**

### **A.1 Cauchy parameterization to determine Polyaniline film thickness**

The Cauchy layer model is commonly used to model transparent materials by spectroscopic ellipsometry. To determine the spectral range where the polyaniline film is transparent, a normal fit was used for the film thickness using two Cauchy parameters  $A_n$ , and  $B_n$ , monitoring the final mean square error (MSE) in the process. When the model is within the transparent spectral range, the MSE of the model fitting will not change significantly by increasing the lower wavelength limit. For the LB-trough EB-PANi film transparent range was at  $>650$  nm.

To avoid any strong correlation between Cauchy parameters, which can result incorrect results, the operator must monitor two things; First, the Cauchy parameters  $B_n$  (and  $C_n$  if used) should not be a large negative number (less than  $-0.01$ ). Second, the refractive index should be physical or consistent with Kramers-Kronig conditions, meaning that within the transparent spectral range the refractive index should not reveal strong dispersion, and should decrease monotonically with increasing wavelength. Figure S.1 is representing refraction index actual measured data for  $5\ 000\ \text{g.mol}^{-1}$  45 layers PANi film.

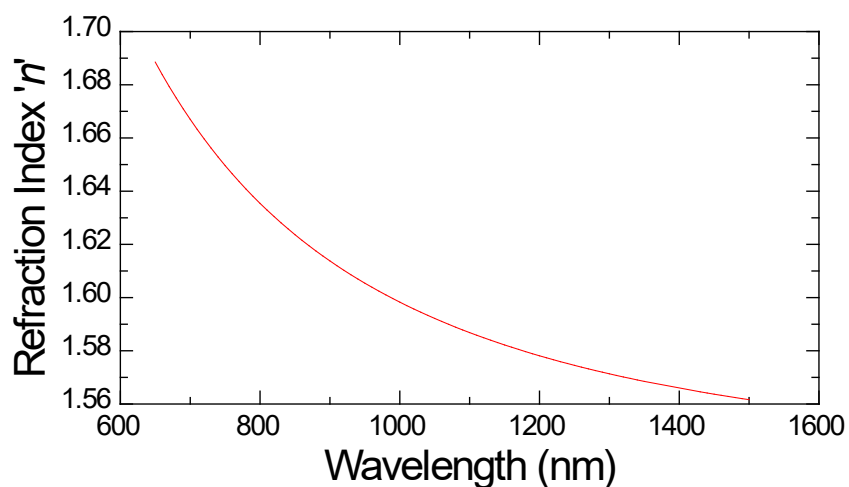


Figure S.1 Refraction index predicted by Cauchy dispersion relation with  $A=1.45$ ,  $B=0.002$ , and  $C=0$ . This is a physically reasonable index spectrum because it decreases by going to higher wavelength indicating not a strong dispersion.

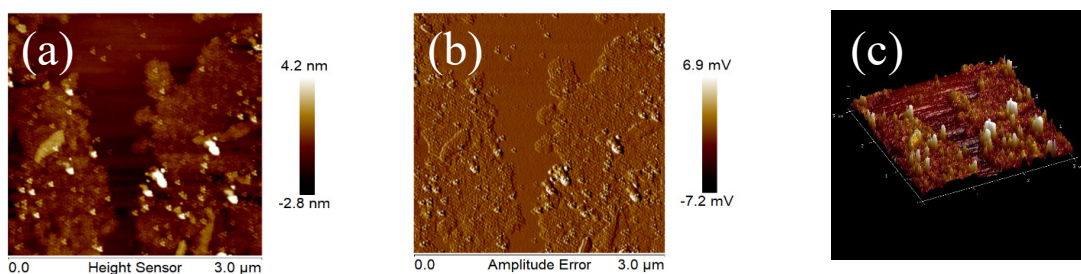


Figure S.2 AFM images of LB-trough EB-PANi 45 strokes, molecular weight = 100 000  $\text{g}\cdot\text{mol}^{-1}$ , DIW subphase and NMP only as the solvent. (a) Height sensor (b) Amplitude error (c) 3-dimensional perspective image

The AFM is used to qualify the surface topology of the LB-trough EB-PANi film deposition on a silicon substrate using the mixture preparation recipe with only NMP as the solvent. The result shows non-uniformity issues for the thin film and domain

boundaries in the size order of 1 to 3  $\mu\text{m}$ . The impact of the NMP on the PANi polymer chain properties requires further investigation.

Table S.1 Detailed LB-trough EB PANi film thickness and surface roughness measurements using AFM and ellipsometry.

NMP + Chloroform (MW=5000 g.mol <sup>-1</sup> )												
SAM#	No of strokes	Step edge	Roughness (nm)				Thickness/stroke (nm)			Doping	Ellipsometry test 1	Ellipsometry test 2
			9 $\mu\text{m}$	3 $\mu\text{m}$	1 $\mu\text{m}$	500 nm	Z type	Y type	Doped Y type only			
1	15	16.6	4.99	4.65	3.91	3.3	2.08	1.11	2.08	NO	12.589±2.5	12.667±2.47
2	15	15.6	5.64	4.67	3.85	2.78	1.95	1.04	1.95	NO	12.565±1.74	12.459±1.86
3	15	16.7	6.23	4.58	3.75	3.3	2.09	1.11	2.09	NO	10.706±0.352	10.207±0.31
4	15	16.2	5.36	3.91	2.98	2.38	2.03	1.08	2.03	NO	10.244±0.182	10.668±0.304
5	15	14.9	6.12	4.86	4.15	2.83	1.86	0.99	1.86	NO	12.811±0.816	13.256±0.616
<b>Average</b>		16.0	5.7	4.5	3.7	2.9	2.0	1.1	2.0			
<b>Standard Deviation</b>		0.8	0.5	0.4	0.4	0.4						
<b>Standard Error</b>		0.3	0.2	0.2	0.2	0.2						
6	45	30.7	9.53	6.37	5.13	3.62	1.34	0.68	1.34	NO	34.667±0.944	32.668±0.887
7	45	25	9.57	7.46	5.32	4.8	1.09	0.56	1.09	NO	24.606±1.09	20.217±1.21
8	45	19.1	10.1	9.52	6.92	4.03	0.83	0.42	0.83	NO	15.406±1.34	16.949±1.55
9	45	28.7	10.5	7.97	5.53	3.79	1.25	0.64	1.25	NO	39.618±1.14	37.850±1.12
10	45	24.6	10.3	8.73	6.33	3.84	1.07	0.55	1.07	NO	28.708±1.15	28.321±1.18
<b>Average</b>		25.6	10.0	8.0	5.8	4.0	1.1	0.6	1.1			
<b>Standard Deviation</b>		4.5	0.4	1.2	0.8	0.5						
<b>Standard Error</b>		2.0	0.2	0.5	0.3	0.2						
11	15	20.9	8.06	7.95	5.27	5.05	2.61	1.39	1.39	YES	21.105±0.235	19.791±0.187
12	15	27.8	9.91	7.88	5.5	4.33	3.48	1.85	1.85	YES	24.630±1.82	24.367±1.95

13	15	23.1	9.45	6.51	3.89	2.22	2.89	1.54	1.54	YES	25.123±2.09	25.272±2.1
14	15	18.1	6.54	6.22	5.08	3.98	2.26	1.21	1.21	YES	15.444±0.77	15.769±0.583
15	15	18.4	8.38	6.11	4.1	2.75	2.3	1.23	1.23	YES	14.016±0.555	14.249±0.519
16	15	29.2	9.66	7.53	5.58	3.26	3.65	1.95	1.95	YES	23.938±0.439	19.701±1.86
<b>Average</b>		22.9	8.7	7.0	4.9	3.6	2.9	1.5	1.5			
<b>Standard Deviation</b>		4.7	1.3	0.8	0.7	1.1						
<b>Standard Error</b>		1.9	0.5	0.3	0.3	0.4						
17	45	93.3	14.3	12.4	6.67	1.51	4.06	2.07	2.07	YES	79.099±0.198	76.805±1.72
18	45	93.5	17	11.1	6.91	4.4	4.07	2.08	2.08	YES	81.058±1.24	83.367±0.468
19	45	95.7	18.3	12.4	5.77	3.4	4.16	2.13	2.13	YES	85.812±1.03	79.322±2.45
20	45	112	19	11.4	6.19	3.68	4.87	2.49	2.49	YES	118.777±1.05	116.585±0.931
21	45	96.4	17.7	13.4	7.51	3.47	4.19	2.14	2.14	YES	115.068±1.01	117.046±1.07
<b>Average</b>		98.2	17.3	12.1	6.6	3.3	4.3	2.2	2.2			
<b>Standard Deviation</b>		7.8	1.8	0.9	0.7	1.1						
<b>Standard Error</b>		3.5	0.8	0.4	0.3	0.5						

The details of the LB-trough EB-PANi film thickness and surface roughness for the molecular weight  $5000 \text{ g.mol}^{-1}$  and using NMP + chloroform as the solvent for two different thicknesses, 15 strokes and 45 strokes, and under two different subphase conditions, neutral DIW subphase and acidic 2M HCl subphase, are provided in this table. The film thickness measurement is in complete agreement with our hypothesis for a Z-type deposition for the undoped film and Y-type deposition for the doped film. A 1.1 to 2.2 nm/layer range was measured using AFM, and spectroscopic ellipsometry, and is also consistent with the literature.